THREE-DIMENSIONAL HEAT TRANSFER ANALYSIS OF A DISPOSABLE, CONTINUOUS-FLOW POLYMERASE CHAIN REACTION DEVICE

by

Victoria Elizabeth Ragsdale

A thesis submitted to the faculty of
The University of Utah
in partial fulfillment of the requirements for the degree of

Master of Science

Department of Mechanical Engineering

University of Utah

May 2012

The University of Utah Graduate School

STATEMENT OF THESIS APPROVAL

The thesis of **Victoria Elizabeth Ragsdale**

has been approved by the following supervisory committee members:

Bruce Gale	, Co-Chair	**02-22-2012** Date Approved
Timothy Ameel	, Co-Chair	**02-22-2012** Date Approved
Carl Wittwer	, Member	**02-22-2012** Date Approved

and by **Timothy Ameel** , Chair of

the Department of **Mechanical Engineering**

and by Charles A. Wight, Dean of The Graduate School.

ABSTRACT

Polymerase Chain Reaction (PCR) is a process which amplifies a specific segment of DNA through a thermal cycling protocol. PCR is largely used in diagnostics, but also has applications in the defense industry and many others. The PCR industry is shifting its focus towards micro-scale devices, and away from macro-scale systems due to i) the micro-scale sample size requiring less blood from patients, ii) total reaction times on the order of minutes opposed to hours and iii) the cost advantages as many microfluidic devices are manufactured from inexpensive polymers. In general, polymers have many advantages including minimal microfabrication processes during manufacturing, wide availability and low cost.

This work presents the manufacturing process as well as simulations and testing results of a disposable polycarbonate (PC) device capable of achieving PCR in less than 7 minutes by thermally cycling the sample through an established temperature gradient in a serpentine channel. This device also features a unique laser manufacturing process eliminating the need for a microfabrication facility. Two-dimensional (2D) and three-dimensional (3D) simulations were created to analyze the heat transfer and fluid dynamics throughout the device. Simulations were created both in the flow plane, to analyze the reaction temperatures occurring in each bend of the serpentine channel, and the out of flow plane, to observe the amount of heat leaving the system. Although the 2D simulations did not produce the same values as the 3D models, the same trends were

exhibited so qualitative observations could still be made. Experiments were performed to validate the simulations by comparing the measured device surface temperature from an IR camera to those values from the 3D simulations. It was found that the device produces fluid temperature results within the reaction limits for several flow rates with specific heater temperature settings. An end point PCR melting analysis was also completed on reactants to determine if PCR was achieved. These results were unsuccessful, due to highly inconsistent flow rates observed during the experiments. Although PCR was not achieved, with slight changes to increase flow rate accuracy, PCR is expected to be successful since the IR images suggest that the fluid is reaching the reaction temperatures.

TABLE OF CONTENTS

NOMENCLATURE

A	Cross-sectional area
A_s	Surface area
c	Specific heat capacitance
D_h	Hydraulic diameter
g	Gravitational constant
h	Heat transfer coefficient for convection
k	Thermal conductivity
Nu	Nusselt number
P_{wet}	Wetted perimeter
q	Heat loss
q''	Heat loss per unit area
Ra	Raleigh number
Re	Reynolds number
T	Temperature of device or body of interest
t	Air gap thickness
T_i	Initial temperature
T_∞	Ambient temperature
T_{surr}	Surrounding Temperature

V	Velocity
$\dot{V}$	Volumetric flow rate
$\forbidden{V}$	Volume
x	Distance in x-direction; direction of isothermal lines in flow plane
y	Distance in y-direction; direction through thermal gradient in flow plane
z	Distance in z-direction; direction normal to flow plane

Greek

α	Thermal diffusivity
β	Volumetric thermal expansion coefficient
ε	Emissivity
μ	Dynamic viscosity
ρ	Density
σ	Stefen-Boltzman constant
τ	Time

ACKNOWLEDGEMENTS

The research performed in this work would not have been possible without the support of my advisors, colleagues and friends. I would like to thank my co-advisors, Dr. Gale and Dr. Ameel, for imparting portions of their vast knowledge of microfluidics and heat transfer to me. Dr. Wittwer has also been invaluable with his expertise in PCR and willingness to let us use his lab to perform our PCR analysis. I would also like to thank Michael Skinner who went out of his way to help me succeed by introducing me to the fastest computer available and was always available to bounce ideas off of. Thank you also to Vishal Nageshkar who perfected the art of the laser and heat press over the summer. Lastly, thank you to my wonderful family who has always been a source of constant support and motivation.

CHAPTER 1

INTRODUCTION

Polymerase Chain Reaction (PCR) is a highly effective and well-established technique to amplify specific segments of DNA. PCR is largely used as a tool for diagnostics in the medical industry but can also be used for paternity testing [1] and detection of airborne pathogens [2-3]. PCR consists of three consecutive reactions: denaturation, annealing and extension. Denaturation occurs when the double-stranded DNA (dsDNA) is heated to a temperature where the double helix is no longer able to keep its shape, usually between 90°C and 96°C [4], causing it to unravel into two single-stranded DNA (ssDNA) segments. The second reaction, annealing, occurs between 58°C and 65°C [4], allowing a single-stranded primer to attach to the ssDNA and identify the location to start replication. Third, extension occurs when a DNA polymerase enzyme, such as *Taq* polymerase, moves along the DNA segment and attaches nucleotides to create a complimentary DNA strand. Each polymerase has a temperature range at which it is most effective, so it can be difficult to determine a generalized ideal temperature range for this reaction. A common enzyme, *Taq* polymerase, is effective between 70°C and 74°C and is generally conducted at 72°C [5]. These three reactions are components of one PCR cycle. In order to obtain useful results, 25-40 cycles are generally required. In

addition to achieving these temperatures, each reaction requires a residence time at the desired temperature to ensure the entire reaction has been completed. Generally the residence times for denaturation, annealing and extension have ratios of 1:1:3 or 1:1:2, resulting in a total cycle time of 4-5 minutes.

1.1 Literature Review

Traditionally macro-PCR is accomplished by thermal cycling a large sample between the reaction temperatures in a controlled environment. The sample includes the DNA, nucleotides and DNA-specific primers and polymerases. Due to the large thermal mass of the PCR mixture, a considerable amount of time is spent changing the entire mixture temperature as it cycles through the reaction temperatures. The required residence times cause this process to be very time consuming. Traditional PCR on a hot-plate type system takes between 1-2 hours for 30 cycles, though more modern air heated systems, such as Roche's LightCycler, can perform 30 cycles in about 15-20 minutes. Over the past decade, the trend has changed from traditional macro-PCR to micro-PCR for several reasons. First, micro-PCR devices require smaller sample volumes, reducing the total reaction time and increasing patient comfort since only a small sample of DNA is needed. Second, micro-PCR devices require less material, reducing the overall cost of raw materials. Third, many can be manufactured using batch microfabrication techniques which reduce the time for manufacturing. Fourth, micro-PCR devices require fewer reagents to complete the same process as macro-PCR devices, significantly reducing the overall cost of the process.

There are three predominant methods for micro-PCR: well-based, shuttle and continuous-flow. Each is characterized by small sample volumes, relatively fast reaction times and microfabrication manufacturing techniques. Well-based PCR houses the reagents in a micro-volume well and the environment temperature changes to complete the cycle. Shuttle and Continuous-flow PCR are accomplished by moving the sample between isothermal regions.

1.1.1 Well-based PCR

Well-based PCR is essentially a direct miniaturization of macro-PCR and was the pioneer of micro-PCR devices. The PCR sample is separated into micro-volume wells, then the entire system is cyclically heated and cooled between the reaction temperatures allowing for required residence times. The accepted heating methods are moving warm air around the reaction chambers [6], a Peltier heater [7-8] or directing an infrared source such as a tungsten or halogen lamp on the wells [9-10]. Systems are normally cooled by either forced convection arising from a fan or compressed air, or by a Peltier cooler. As these systems have been created and improved upon, progress has been made to increase the number of reaction wells and achieve better temperature control.

The number of PCR reaction chambers is limited only by the heating and cooling capacity of the array. Systems with up to 37 wells have been successful using a LabView-controlled Peltier stage for temperature control [7]. Systems using infrared sources to modulate the temperature have produced successful results with 6 and 7 radially axisymmetric wells [9-10]. These IR-mediated thermally controlled systems have fewer allowable wells, due to the limited homogenous temperature area IR sources can produce.

Traditionally, well-based PCR is accomplished in glass capillaries [6, 11-12] and polypropylene (PP) tubes [13], but has also been demonstrated in glass-silicon hybrids [8, 14] and a variety of polymers including polycarbonate (PC) [7], poly-methylmethacrylate (PMMA) [10] and Polyester-toner (PeT) [9].

Advantages to well-based PCR include a simple test set-up, since no specialized equipment is needed for the PCR reactants, and many different samples can be processed simultaneously. On the other hand, heating and cooling the fluid takes a considerable amount of time since the entire container must first be heated, then time is needed to ensure the entire micro-volume reaches the reaction temperature. Although well-based PCR is used in industry, the next two presented methods have been shown to accomplish PCR with faster process times, less time in temperature transition and better temperature control.

1.1.2 Shuttle PCR

In order to reduce the time waiting for fluid temperatures to transition between reactions, shuttle PCR was created. Shuttle PCR allows a micro-volume of PCR reactants to move between three isothermal regions in a single channel. This eliminates the need to heat a container and allows the dwell times and velocity between isothermal zones to be controlled independently, which makes the system adaptable to any length of DNA or polymerase. Figure 1.1 shows a general schematic of a shuttle PCR system.

Since the isothermal regions remain at the desired temperature and the sample generally has a very small volume, the time for the sample fluid to reach the reaction temperatures is low. Chen *et al.* [15] produced a system with a cycle time of 65 seconds,

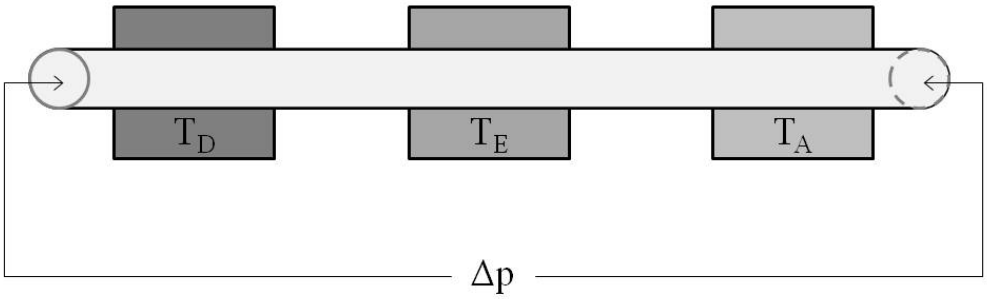

Figure 1.1: Schematic of a shuttle PCR system. Three isothermal regions are established, T_D, T_E and T_A. Each corresponds to the denaturation (T_D), extension (T_E) and annealing (T_A) temperatures.

but with a sample volume of 2μL. As presented in another publication, Chiou *et al.* [16] designed a system which used a sample volume of only 1μL, achieving a cycle time of 16 seconds. Both of these systems housed the sample in a glass capillary and shuttled the sample plug over different steady state heaters.

Cheng *et al.* [17] used a sample volume of 100 μL and an established radial temperature gradient. Two concentric Indium Tin Oxide (ITO) heaters were arranged on a chip and a microchannel was machined into PMMA in such a way that the sample followed the isothermal lines for the required residence times then moved radially outward to get to the next desired isothermal line.

Shuttle PCR is able to produce reliable amplification results while completing the process faster than well-based PCR, but it relies heavily on specialized MEMS pumps and valves, which are expensive, to control the location and acceleration of the fluid and is only capable of cycling one sample at a time.

1.1.3 Continuous-flow PCR (CF-PCR)

Continuous-flow PCR (CF-PCR) uses pressure driven flow to continuously move a PCR sample in one direction through three temperature regions with a constant flow rate. There is no need to heat or cool a container and the equipment needed is basic and simple to operate. In general, a serpentine channel is passed through isothermal regions as shown in Figure 1.2.

Kopp first showed CF-PCR by passing a constant width microfluidic channel through three distinct temperature regions. The channel geometry was designed to allow more time to occur in the extension temperature region [18]. This design was improved by Schneega *et al.* by including additional insulation to isolate the desired temperatures more efficiently [19]. Li *et al.* [20] varied the width of the channels allowing regional velocity control. Therefore, velocity was faster during the transition temperatures and slower through the extension phase.

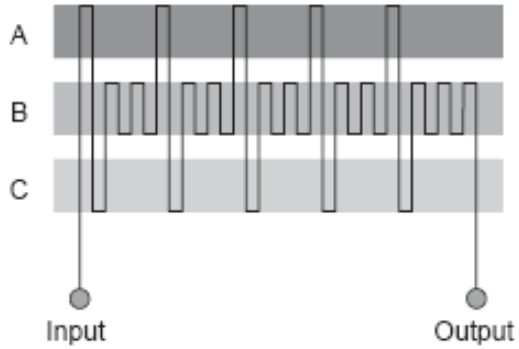

Figure 1.2: A schematic of a CF-PCR device. Three temperature zones are defined as A,B,C which are associated with denaturation, extension and annealing, respectively. Notice the geometry in the extension phase is longer to increase the residence time and ensure the entire reaction is completed before continuing on.

Not all CF-PCR systems have followed the geometry presented in Figure 1.2. Success has been documented in systems with a spiral channel design. Hashimoto *et al.* [21] developed a one-plane CF-PCR device which spirals the PCR mixture through isothermal regions. Park [22] and Dorfman [23] projected this one-plane geometry into a cylinder where the temperature regions were defined lengthwise along a cylinder. The PCR mixture flowed through a tube which was wrapped around the heater blocks. This design allowed for a constant time at each temperature anywhere during the process, unlike the first design.

Simplifying the design back to one plane, Chen *et al.* [24] designed a CF-PCR device which pumped a PCR sample continuously through a single square channel where isothermal regions at the desired temperatures were established below the channel. This design allowed the unique opportunity for a continuous-flow device to vary the number of cycles and residence times in order accommodate any DNA fragment length.

Thus far, the systems presented have all relied on the ability to establish isothermal regions and dwell times to insure the entire reaction has been completed. Wittwer discovered that denaturation and annealing occur almost instantly (less than 1 second) once the required temperature is reached [25]. Wittwer *et al.* also found that no residence time is required in the extension phase if the DNA segment of interest is less than 200bp [25]. Returning to the traditional CF-PCR design, Crews *et al.* [26] created a successful CF-PCR device from glass based upon these principles which passed the fluid through an established temperature gradient and required little to no residence times. The serpentine channel is wound through a temperature gradient created by two heaters, but did not extend the channel length during the extension region, like its predecessors. The

channel width was simply increased through the extension phase temperatures, which decreased the velocity enough to give the PCR mixture time to fully complete the extension process. Orozco [27] then expanded on this work and completed an extensive finite element study to show the effects of flow rate, entrance/exit effects, channel spacing, material, and environmental effects such as ambient temperature and convection effects.

CF-PCR has been shown to work effectively with a constant flow rate and an established temperature gradient. This process does not require specialized hardware since the fluid is pressure-driven. It also lends itself to *in-situ* fluorescence to monitor the PCR progress during experimentation. One disadvantage of CF-PCR is that the number of amplification cycles and residence times are determined during the fabrication process. This means each device must be designed for a particular range of DNA segments and polymerases. However, this could also allow the geometry to be optimized for a particular segment of DNA, so the process would be as efficient as possible, wasting no time. As with the two previous methods being limited by the residence times, continuous-flow devices are limited by flow rate. As the flow rate is increased, the effectiveness of PCR is reduced since the PCR mixture is not given ample time in each temperature zone to complete the reaction. Despite these minor disadvantages, CF-PCR is able to achieve rapid amplification rates while producing a highly effective output with minimal instrumentation. The device developed in this thesis relies on this continuous-flow concept.

1.2 Manufacturing and Materials

Two factors must be considered when determining a material to use for a micro-PCR device. The first is the availability and cost of the raw material and associated manufacturing costs. The second arises from the surface effects associated with the high surface-to-volume ratios exhibited in microfluidic channels. These dominating surface effects include enzymes "sticking" to hydrophobic surfaces and enzymes being adsorbed to the channel walls, both of which inherently reduce PCR efficiency. Two methods for reducing these effects are including additives in the PCR mixture and treating the channel surfaces. Therefore, the second consideration when choosing a material for PCR is determining which preventative processes are associated with the material to reduce these surface effects.

Glass has historically been used to create micro-PCR devices due to its predictable thermal behavior, known surface chemistry, and wide-spread availability. Schneega [19] and Crews [26] etched microchannels into glass to give the channels smooth and rounded edges. However, the manufacturing process associated with glass requires specialized micromachining equipment and is costly both in time and resources. The typical process for etching glass includes sputtering a thick film of chromium onto the glass blanks, spinning a layer of photoresist on that chromium layer and patterning it using standard mask lithographic procedures. After a hard bake, the glass is exposed to a chromium etch which removes the metal where the channel will be etched. A protective backing to the glass is applied, then the slides are immersed in an HF etchant bath until the desired depth is achieved. Inlet and outlet holes are carefully drilled using a diamond tipped drill bit. Once the slides with the channels are cleaned, they are anodically bonded

to a blank glass slide using temperature, pressure and time [28]. This process takes about an entire day. It should also be noted that with batch fabrication, the manufacturing time per device can be reduced. However the bonding, drilling and fluidic connections must be done individually for each device.

The glass channel walls are naturally hydrophilic, lending themselves to enzyme and DNA adsorption. In addition to this laborious manufacturing process, further steps must be taken to increase surface passivation. If no additional surface modification is completed, PCR will not be successful [18-19, 22]. The channel walls must be coated with a silanizing agent to make the channel walls hydrophobic. Such silanizing agents include hexamethyldisilazane (HMDS) [19], dimethyldichlorosilane (DMDCS) [15], and N,N-dimethylformamide (DMF) [29]. Additives, such as Bovine Serum Albumin (BSA), can also be included in the PCR mixture to prevent surface denaturation of polymerase in glass channels [19].

Veering away from the fragility of glass and increasing heat transfer to the fluid, microchannels were manufactured in highly conductive silicon wafers, then bonded to a flat glass slide. The manufacturing process is similar to that of glass in that a microfabrication facility and standard photolithography processes are required. However, due to the fact that silicon inhibits PCR, a method for preventing silicon reacting with PCR was required. Shoffner [8] researched several methods to overcome this and found that the PCR inhibition can be removed by either coating the channels with a silanizing agent, such as SurfaSil, followed by a polymer coating, such as poly-a-alanine, or thermally oxidizing the channel. The latter provided consistent results due to the ability to consistently achieve a uniform silicon oxide (SiO_2) layer.

Due to the costs and challenges associated with glass and silicon manufacturing, there was a movement in the PCR industry to manufacture devices from polymers. Polymers are inexpensive and can be manufactured more quickly than glass, primarily because a mold is generally used to make multiple parts rapidly. This mold is usually the only part which must be manufactured using microfabrication techniques. Once the mold is created, each device can be made outside a microfabrication facility. However, polymers naturally absorb hydrophobic materials, so greater attention is required to increase surface passivation. The two most common polymers used in microfluidic devices are polydimethylsiloxane (PDMS), and polycarbonate (PC) but has also been shown effective in PMMA [10, 17], Polyester-Toner (PeT) [9], and Zeonex [30].

PDMS is a flexible, transparent polymer which is created by mixing 10:1 liquid PDMS and curing agent. Traditionally, channels are created in PDMS by exposing a silicon wafer with negative photoresist on the surface to UV light through a chrome mask with the channel pattern. The wafer is then developed and the PDMS mixture is spun onto it, allowed to bake, then removed from the silicon wafer, revealing the channels created by the negative resist structures and bonded to another piece of solid PDMS. Although this method eliminates the need for glass etching, it still relies on standard micromachining practices for each device even though multiple devices could be made from one silicon wafer. Challenges associated with PDMS are gas permeability and swelling that can both induce bubble formation and sample evaporation and leads to PCR failure. Shin *et al.* [31] found that a Parylene coating used in a PDMS channel prior to the addition of PCR reagents provided sufficient protection to the proteins and also reduced

bubble formation. Kim *et al.* [32] used polyvinylpyrrolidone (PVP) as a dynamic coating to inhibit enzyme adsorption.

Polycarbonate (PC) has a very low thermal conductivity, about 10% that of glass, and has advantages in creating isothermal regions, but creates challenges with transferring heat into the fluid. A PC channel developed in 2005 [24] was created through a hot embossing procedure. A micromachined brass mold was manufactured using traditional microfabrication steps, then heated and pressed into the PC substrate. The system was allowed to cool and the mold was removed. The channel was created by thermally annealing another PC substrate on top of it. To modify the channel chemistry, a dynamic Polybrene coating was applied to the channel surface.

Although PCR conducted in continuous-flow microfluidic channels requires additional surface passivation techniques, many methods have been researched and proven to overcome this problem. It has also been shown that progress has been made to reduce the need for micromachining processes in the creation of PCR devices; however, this work will present a process that completely eliminates these microfabrication steps.

1.3 Motivation and Objective

The device presented in this thesis relies heavily on the principles established by Crews with his serpentine channel glass device. Such principles include the ability to create an established temperature gradient and move the PCR reactants through a varied width serpentine channel to reach the reaction temperatures while achieving regional velocity control. As previously discussed, however, the manufacturing of glass devices is time consuming and expensive. Laser ablation is a relatively new and versatile

manufacturing process used with many polymers. In short, laser ablation cuts microchannels out of a polymer with a CO_2 laser which makes multiple passes until the channel geometry has been completely removed from the bulk material. This layer is then bonded between two solid layers to create the channel. This method completely eliminates the need for a microfabrication facility.

Using this new manufacturing technique and the theory behind Crews' device, a CF-PCR device created in PC is presented which completely eliminates the need for a microfabrication facility. Changing the material from glass to PC appears to have thermal isolation advantages, but it is unclear how this material will affect the temperature gradient, react with the PCR reaction mixture, and respond to environmental variables such as convection.

The objective of this work is to show that PCR can be achieved in a disposable, continuous-flow, polycarbonate device, manufactured using a simple and cost-effective laser process, through finite element simulations and validated by several experiments. In addition to these findings, a thermal analysis of the heat lost from the device is conducted and means of reducing these effects are presented.

Chapter 2 will discuss the design, theory and manufacturing of the device. The methods and results from a flow plane simulation are presented in Chapter 3. This model focuses particularly on whether the reaction temperatures can be achieved in PC and how well the temperature gradient can be established. Chapter 4 will detail an analysis of the out of flow plane heat transfer. The experimental validations of the simulations are detailed in Chapter 5. Lastly, a summary of findings and conclusions, as well as a future work discussion, will be given in Chapter 6.

CHAPTER 2

DEVICE DESCRIPTION, THEORY AND MANUFACTURING

Microfluidic continuous-flow PCR devices are gaining greater recognition in the PCR industry as many have been shown to amplify DNA as well as commercial PCR machines and with shorter total reaction times. Many of these devices are manufactured from polymers and can be produced quickly and in large volumes. This chapter will discuss the proposed device in detail and present the microfluidic and heat transfer equations used to characterize the device behavior. The complete microfabrication-free manufacturing procedure is also discussed.

2.1 Device Description

The device proposed in this work is based on the design by Crews et al. [26], and instead of being made in glass, the device is made in polycarbonate. As with Crews' device, the disposable device proposed in this article is designed to amplify DNA using principles of continuous-flow thermal gradient PCR, which is characterized by thermally cycling a sample as it travels through an established temperature gradient. Compared to the Crews' device, the PC device is also designed to be cost effective and simple to manufacture.

2.1.1 Device Geometry

As the proposed device relies on a continuous-flow PCR design and a fixed geometry, the number of PCR reaction cycles must be determined during the design process and cannot be changed after manufacturing. Since reliable PCR results are obtained between 20 and 40 cycles, the device is designed with 25-cycles to give the smallest device footprint possible while still generating reliable results. In this serpentine channel, one cycle is defined from one denaturation temperature to the next, or geometrically from peak to peak.

Continuous-flow PCR implies the fluid is given a constant volumetric flow rate, and since the PCR sample requires more time in the extension phase than in the denaturation and annealing phases, the channel width is varied to allow for regional velocity control since the channel height must remain constant. The dimensions are selected to produce the same channel volume as Crews' device. The channel is given a constant width of 0.5 mm when the sample is traveling from denaturation to annealing and 1.2 mm through the extension phase. The neighboring fluid channels are spaced 0.8 mm apart, resulting in the fluid traveling a distance of 0.033 m each cycle. Allowing for an approximate 10 mm window of material around the channel geometry, the device footprint area becomes 103.3 x 32.3 mm and is shown in Figure 2.1. The total thickness of this device is approximately 0.33 mm so the channel height is predicted to be 0.11 mm. With the proposed geometry and a standard flow rate of 1 mL/hr, a cycle time of 15 seconds is expected.

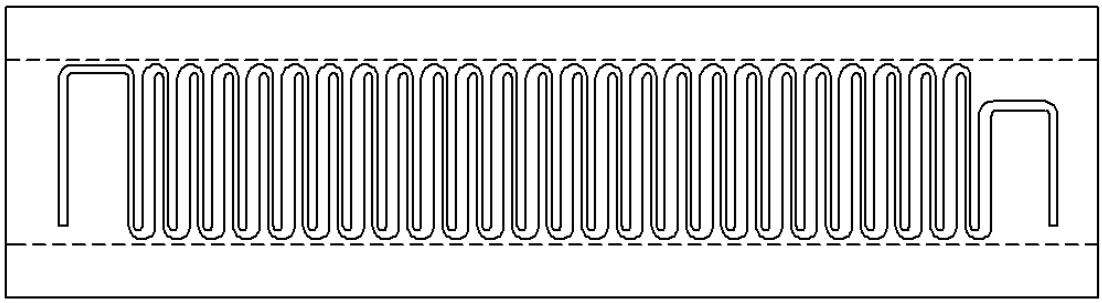

Figure 2.1: Flow plane geometry of CF-PCR device. The fluid is inserted on the left side then travels through the channel and exits on the right. The dashed lines represent the proximity of the heaters to the fluid channel.

2.2 Device Design Theory

2.2.1 Material

The proposed device is made from polycarbonate (PC) sheets (Lexan FR83). PC was chosen due to its relatively low cost, ease of manufacturing, transparent properties and low thermal conductivity. In the past, materials with very high thermal conductivity k, such as silicon (k = 149 W/m-K), have been used in PCR devices which rely on quick heat transfer into the fluid, thereby reducing the amount of time spent waiting for the sample to reach the reaction temperature. Although this process is very important to shuttle PCR systems, and has some importance in continuous-flow systems, the proposed continuous-flow PCR device primarily relies on its ability to establish a consistent temperature gradient across the chip. A material with low thermal conductivity, such as PC (k = 0.20 W/m-K), is more likely to be able to maintain a consistent temperature gradient. Although establishing a steady state temperature gradient will take more time, it will not be as affected by environmental conditions or fluid motion when compared to a material with high thermal conductivity. Also because the device is so thin, a steady state

temperature gradient can be established more quickly because the heat travels perpendicularly from the heaters directly into the fluid channel without heating much material out of the flow plane.

In addition to the thermal advantages, the PC laminate is available in opaque and transparent films, both of which are used in the device. The bottom layer is opaque, providing a consistent background for flow visualization, while the center and top layers are transparent, allowing the potential for real-time fluorescent imaging of the PCR as the sample travels through the device.

2.3 Device Design Theory

The PCR reactants are able to amplify DNA if the sample is thermally cycled following standard PCR protocols, which were discussed in Chapter 1. This device accomplishes PCR by first allowing the fluid to enter and reach the denaturation temperature (90-96°C) so the double-stranded DNA (ds-DNA) can no longer hold together and splits into two single-stranded DNA (ss-DNA). The fluid then quickly travels down the channel to the annealing temperature (58-65°C) where primers are attached to the ss-DNA. The ramp rate between denaturation and annealing can happen as fast as the fluid temperature can change, hence the smaller channel width in this region. Also, for most DNA segments, these reactions are completed instantaneously once the reaction temperature is reached. The sample continues around the 180° bend and, as it moves back through the thermal gradient, the DNA polymerase seeks the primer locations and begins adding extra nucleotides to the ss-DNA, producing a new ds-DNA. Although the extension rate is optimal at an enzyme-specific temperature (72°C for Taq

Polymerase), the reaction is able to occur through a larger temperature range (70-75°C) [4]. This extension reaction may take several seconds to complete for longer DNA target regions; however, it has been shown to occur nearly instantaneously in DNA segments consisting of less than 100 base pairs (bp). In order to account for this wide range of possible reaction times, the channel width is increased to allow adequate time for the reaction to complete before starting the next PCR cycle. This device is designed to perform PCR for an unknown DNA segment length; however, if the DNA length is known, the device cycle time could be significantly decreased by optimizing the channel width to only become wider during the most efficient extension temperatures.

2.4 Theory

The device relies on the principles of fluid dynamics in micro-sized channels and heat transfer, primarily conduction into the fluid. In order to fully understand how the device operates, an understanding of these subjects must first be achieved.

2.4.1 Microfluidics

Microfluidics is defined as the science and engineering of systems in which fluid behavior differs from conventional flow theory primarily due to the small length scale of the system [33]. In contrast to conventional flow theory which concentrates primarily on the study of turbulence, microfluidic flow is characterized almost entirely by laminar flow. In flow through a channel, laminar flow has a velocity component only in the direction of the flow, whereas turbulent flow has velocity components in all 3 directions, which make it very difficult to predict. Microfluidic flow calculations are therefore

considerably easier than macro-scale flows due to the predictability of laminar flow. It is important to note, however, that the no-slip condition seen in macro-fluidics is still applicable with this small length scale.

Determining whether flow is turbulent or laminar depends solely upon the Reynolds number.

$$Re = \frac{\rho V D_h}{\mu} \quad [2.1]$$

For a square channel, the hydraulic diameter, D_h, must be used as the length scale and is defined as:

$$D_h = \frac{4\,A_c}{P_{wet}} \quad [2.2]$$

In an enclosed channel, if *Re* is less than 2300, the flow is considered laminar [34]. In order to reach a *Re* larger than this value, the velocity would have to be very fast, the density would have to be very large, or the dynamic viscosity would have to be very small. With micro-devices being considered, the hydraulic diameter will be on the order of 10^{-4} and the fluid mixture generally used can be approximated by water, which has a density of approximately 1000 kg/m^3 and a dynamic viscosity of approximately $1\text{x}10^{-3}$ N-s/m^2. For the flow to be outside the laminar region, the velocity would have to be approximately 20 m/s, which is unrealistic.

Microfluidic governing equations include conservation of mass, momentum and energy. If an incompressible, steady state, Newtonian, isotropic channel flow with

negligible viscous dissipation and body forces is being considered, the governing equations become:

$$\frac{\partial u_i}{\partial x_i} = 0 \quad [2.3]$$

$$\rho\left(u_i \frac{\partial u_i}{\partial x_j}\right) = \frac{\partial P}{\partial x_i} + \frac{\partial}{\partial x_i}\left[\mu\left(\frac{\partial u_i}{\partial x_j} + \frac{\partial u_j}{\partial x_i}\right)\right] \quad [2.4]$$

$$\rho c_v\left(u_i \frac{\partial T}{\partial x_i}\right) = \frac{\partial}{\partial x_i}\left(k \frac{\partial T}{\partial x_i}\right) \quad [2.5]$$

It can be assumed that the flow observed in the channel will be laminar. As the flow rate increases, there is less time for the fluid to absorb the heat from the surrounding device; therefore, a higher heater temperature setting will be required for faster flow rates.

2.4.2 Heat Transfer

There are three modes for heat to transfer: (i) conduction, (ii) convection, and (iii) radiation. Conduction is characterized by heat transferred between two materials that are physically in contact. Convection is the heat transferred from a surface to the surroundings based on a temperature difference and fluid motion. Radiation is the energy that is emitted from matter at any non-zero temperature and does not require any medium to transfer this energy. All three modes are important to microfluidic devices. Conduction moves heat from the heaters through the device and into the fluid, convection removes heat from the top of the device and its value varies with ambient temperature and

surrounding fluid motion, and radiation causes energy to be emitted to the surroundings from the top surface [35].

2.4.2.1 Conduction

Conduction is the most dominant form of heat transfer in any PCR device and is solely responsible for achieving required temperatures to complete the PCR reaction. Since temperature control is arguably the most important design aspect of a PCR device, it is imperative to have a basic understanding of the governing conduction equation, known as Fourier's Law.

$$q = -kA\frac{\partial T}{\partial x} \qquad [2.7]$$

The negative sign simply indicates that heat will move from warmer regions to cooler regions. Conduction is dependent upon the thermal conductivity of the material, the cross-sectional area and the temperature difference between the current and desired temperatures.

2.4.2.2 Convection

Although convection is present and desirable within the fluid channel, convection on the top of the device removes heat from a system and is undesirable for PCR devices. The rate of heat transfer increases as the movement of surrounding air increases and as the temperature difference between the environment and the device increases. This is expressed mathematically by Newton's Law of Cooling.

$$q = hA_s(T - T_\infty) \quad [2.8]$$

The convection coefficient, h, represents the air movement and A_s is the surface area that is losing heat. This effect can be reduced, and even eliminated, by encasing the device in a protective case removing all external fluid motion over the device. Under specific conditions, however, natural convection can be initiated in an enclosed area. Newton's Law of Cooling still applies, but the convection coefficient is determined from the Nusselt correlation:

$$Nu = 1 + 1.44\left[1 - \frac{1708}{Ra_L}\right]^+ + \left[\frac{Ra_L^{\frac{1}{3}}}{18} - 1\right]^+ \quad [2.9]$$

and

$$h = \frac{Nu\ k}{t} \quad [2.10]$$

Note that $[\ ]^+$ denotes the term should only be included if the value is positive; set to zero if negative. The Raleigh number is defined in Eq 2.11.

$$Ra = \frac{g\beta(T_{hot} - T_{cold})t^3}{\alpha\nu} \quad [2.11]$$

where g is the gravitational constant, 9.81m/s^2, β is the thermal expansion coefficient and is 595.4E-6/K at a temperature of 345K [35].

Convection is observed in an enclosure if the Raleigh number (*Ra*) is greater than 1708 [35]. Since *Ra* is proportional to temperature and enclosure distance and inversely proportional to the gas properties, the only parameter that can be varied is the chamber thickness. Figure 2.2 represents a plot of the Raleigh number as a function of enclosure distance. From this plot, and validated by hand calculations, the distance at which *Ra* is equal to 1708 is slightly greater than 6 mm.

This enclosure natural convection phenomenon is observed in Figure 2.3. These figures show how the evidence of natural convection becomes very clear in gaps larger than 6 mm. Therefore, for enclosures less than 6mm, conduction may be assumed.

2.4.2.3 Radiation

Radiation allows heat to leave or enter a system dependent upon the system's temperature relative to the surroundings. Radiation requires no medium, is usually undesirable and is difficult to control. Radiation heat loss is expressed in Eq 2.12.

$$q = \sigma \varepsilon A_s (T_s^{\,4} - T_{\text{surr}}^4) \qquad [2.12]$$

The only term which can be altered is the surrounding temperature. Therefore, the only way to reduce radiation without changing the material would be to increase the surrounding temperature to a temperature near the device temperature, which is not realistic in a typical lab setting.

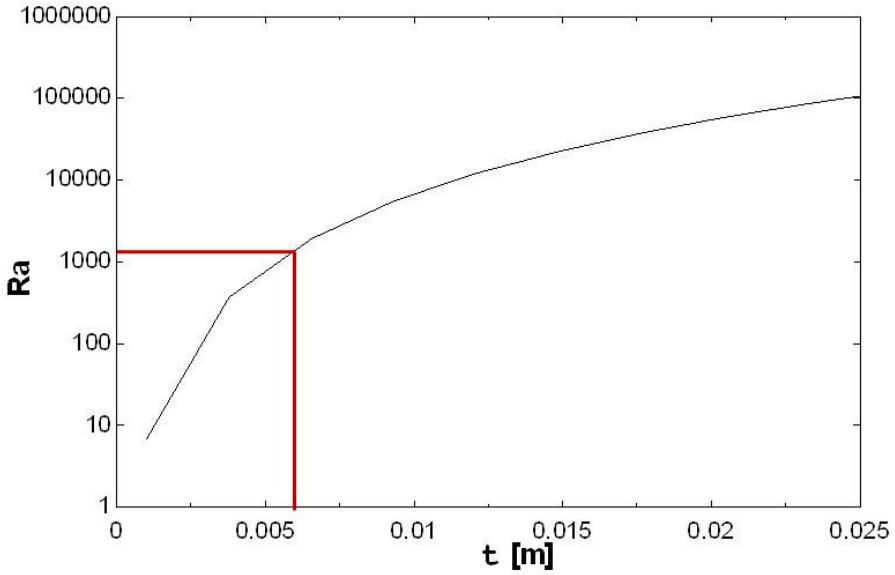

Figure 2.2: Validity of *Nu* correlation used is based on the Raleigh number. As the air gap thickness is increased, a larger *Ra* is observed. A *Ra* of approximately 1704 corresponds to an air gap thickness of approximately 6 mm. Therefore, convection can be assumed to occur in enclosures with a *t* greater than 6 mm.

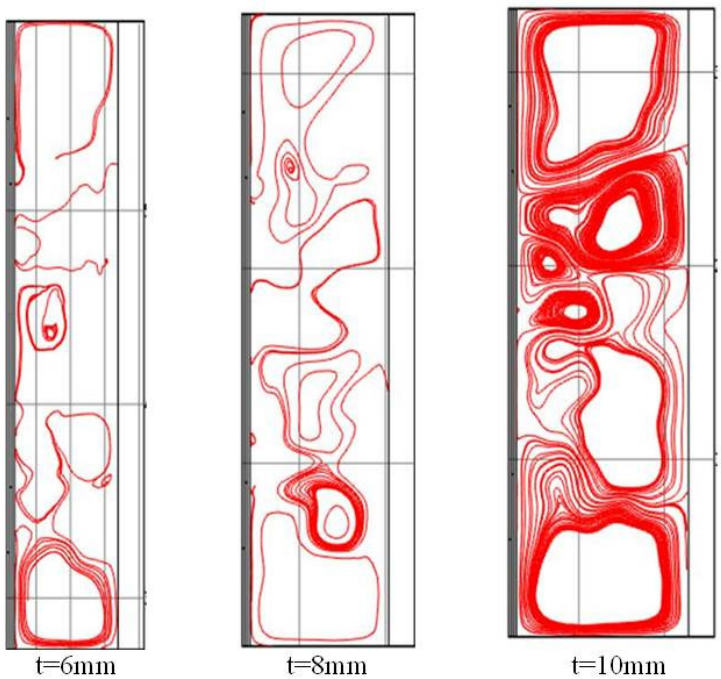

Figure 2.3: Streamlines are plotted in an enclosed region to show how natural convection is created in an enclosure and how its effects are increased with increasing gap thickness. These were created in a 2D COMSOL Multiphysics simulation.

2.4.2.4 Heat Transfer Discussion

When comparing the different heat transfer mechanisms, the only heat transfer mode causing heat loss that can be controlled is convection. So, to reduce the amount of heat lost during this process, efforts must be made to reduce the impact of convection. This will be accomplished by using an enclosure.

2.5 Device Manufacturing

The manufacturing process for the microfluidic devices used in this work is based on a relatively novel laser laminate ablation process which completely eliminates the requirement of a microfabrication facility and traditional microfabrication techniques. The device is manufactured from three layers of polycarbonate. The center layer houses the serpentine channel geometry, making the height of the channel entirely dependent on the thickness of the laminate, while the outside layers provide the top and bottom walls to form the PCR device.

The manufacturing process begins with an appropriately sized piece of PC laminate rolled onto backing tape (Conform 4075-RLA) of roughly the same size to provide stability and protection during the laser procedure. The channel volume is then created in this layer by cutting the channel perimeter with a CO_2 laser (Universal Laser Systems, Versa Laser). The laser is programmed to cut completely through the PC but not through the backing tape. This laser is capable of producing smooth edges while maintaining tight tolerances. Tweezers are used to gently remove the cut-out segment, creating the channel within the bulk material. An equally sized transparent PC layer is placed on top of the created channel geometry with the backing tape still attached to the

other side. These PC pieces are then placed between two pieces of flat, smooth plastic (backing of MacTac 8300p vinyl), placed in a protective Teflon sleeve and laminated for 3 minutes at 175°C in a heat press. The purpose of using the smooth plastic surfaces to surround the device is to prevent defects in the Teflon sleeve being imprinted into the device. After lamination, the backing tape is carefully removed. Inspection is necessary to ensure that the PC layers are firmly laminated to each other. Before the bottom opaque layer may be applied, port holes must be cored allowing fluid access into and out of the channel. Coring is completed by placing the two layer device on a sturdy, yet pliable material, such as PDMS, then gently pushing a coring tool into the inlet and outlet port locations at each end of the channel. The PDMS backing provides support so the hole is uniform and does not create hairline cracks around the edge while also providing a place for the coring tool to go after it penetrates the device. The opaque bottom layer is then laminated in the same manner for about 2.5 minutes at 175°C. Several precautions must be taken when using the heat press, the most important of which is ensuring the top and bottom layers do not bond together in the channel. This bonding is prevented by allowing the layers to be under heat and pressure for no more than 3 minutes each. Another issue that must be avoided is the formation of creases and bubbles created between the PC layers. The creases generally arise if the smooth flat plastic used in the heat process is used more than once. The outline of the previous channel is imprinted into the shielding layer and is then translated into the next device. Therefore, a new shielding layer is recommended for each set of devices made. Bubbles occur when the layers are not completely flat, so it is important to make complete contact when the channel layer is initially rolled onto the backing tape prior to cutting in the laser system.

With the device laminated together and cut into shape, the last step is creating and attaching the nanoports which are required to allow the PCR sample to be injected into the system and easily collected at the end. The PDMS-based nanoports are created by mixing PDMS and a curing agent in a 10:1 ratio, then pouring the mixture approximately 4 mm deep into a petri dish. This mixture is cured for 2 hours at 60°C. The cured PDMS is then removed from the dish and cut into approximately 1 cm x 1 cm squares and set aside. Double-sided pressure sensitive tape (3M 96042) is also cut into 1 cm x 1 cm squares and a 1 mm hole is cored in the center of the tape squares. The tape is then firmly pressed onto the PCR device so that the holes in each tape line up with the inlet and outlet holes. Going back to the PDMS squares, 1 mm holes are cored in the center of the squares in a similar fashion as the tape. Finally, the PDMS squares and the bonding side of the tape are oxidized with air plasma for about 30 seconds each. Then, the PDMS is quickly and firmly pressed against the double-sided tape on the PCR device, using a pin to ensure the holes are aligned. The final device is shown in Figure 2.4.

The entire manufacturing protocol takes approximately 3 hours, including the 2-hour PDMS curing process. The average manufacturing time per device can be reduced further since multiple devices can be cut and laminated simultaneously. This device's glass predecessor took an entire day to manufacture. Using this PC laser lamination process is faster and cheaper both in time and resources.

2.6 Discussion

The most critical component to the success of this device is establishing a uniform thermal gradient along the device so the sample is able to achieve the PCR reaction

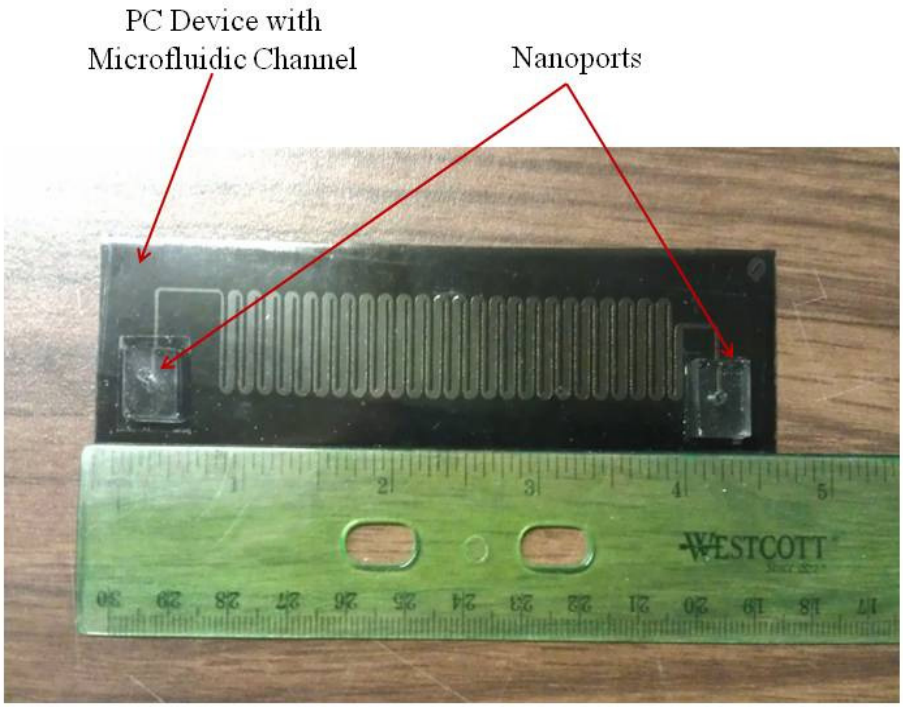

Figure 2.4: The final device with nanoports attached measuring about 4.5 in. in length.

temperatures at each bend. This gradient is directly related to the conduction from the heaters into the fluid channel; however, convection and radiation may also prove vital to the success of the establishment of the temperature gradient.

CHAPTER 3

FLOW PLANE COMPUTATIONAL METHODS AND RESULTS

Simulations of the device, coupling heat transfer and fluid dynamics, are completed both in 2D and 3D, to validate polycarbonate (PC) as a suitable material for PCR. Through this study, observations about the design heater location and entrance length can also be made. Since PC has such a low thermal conductivity, it is important to validate that the fluid sample can reach the required reaction temperatures at various flow rates.

COMSOL Multiphysics Version 4.2 was used to solve all the simulations discussed in this work. This program offers many different 'physics' to simulate real world problems. The physics used for this simulation was 'conjugate heat transfer,' which pairs heat transfer with fluid dynamics, allowing both solutions to be solved simultaneously.

3.1 2D 25-cycle

To gain a first approximation of the fluid temperature within the channel, a 2D simulation of the device is conducted through the flow plane with a very slow fluid flow rate.

3.1.1 Boundary Conditions

The geometry with applied boundary conditions, as shown in Figure 3.1, indicate that the device areas in contact with the heaters above and below the fluid channel have been removed. This is justified by noticing that in a 2D simulation, the heater temperatures may be defined as the area above and below the fluid channel; however, only the line interface between the heater and the device is necessary. The heater temperatures are then defined on the boundaries above and below the channel and the flow is given an inlet velocity representative of a particular flow rate. The outlet is given a reference pressure of zero. Any boundary without a specified temperature is considered to be adiabatic. An important feature in the 2D COMSOL workspace is the option to use a 'shallow channel approximation.' When this option is selected, the device thickness must be defined and the simulation is solved in pseudo-3D space. Without this feature, the velocity profile produced in 2D is not what is observed in 3D. To accurately represent the velocity, this feature must be selected.

The specific boundary conditions are the denaturation and annealing heater

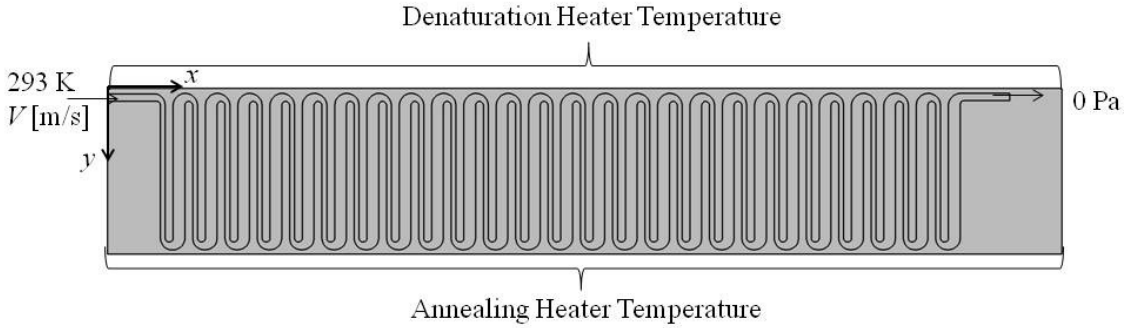

Figure 3.1: Boundary conditions for a 2D simulation with 25-cycles.

temperatures defined as 370K and 323K, respectively, an inlet velocity of 0.00023 m/s representing a flow rate of 0.1 mL/hr, and the shallow channel approximation was given a device thickness of 0.00011m.

3.1.2 Mesh Refinement and Convergence Criteria

In simulations where both fluid dynamics and heat transfer are being analyzed, the fluid velocity is more sensitive to the mesh size than temperature since the velocity varies much more than temperature across the width of the channel. A fine enough mesh must be created to capture the no-slip condition at the walls yet still express an accurate maximum velocity in the center. The mesh used to solve this problem has 265402 mesh elements. The maximum velocity for fully developed flow simulated with this mesh was compared to a similar solution for a mesh with 320785 mesh elements; a 0.2% error was generated when compared to the solution with the more refined mesh. Although no rule of thumb exists for acceptable error in numerical simulations, the simulation solutions presented in this thesis are assumed to be mesh independent if the relative error between two meshes is less than 2%.

The convergence criterion was defined as the velocity, temperature and pressure changing less than .001 units between iterations. Also, if the simulation did not converge in 100 iterations, an error was indicated and the simulation terminated. Using this convergence criterion, the solution is assumed to be fully converged.

3.1.3 2D 25-cycle Results

Upon solving this 2D problem, the plots in Figures 3.2 and 3.3 are produced representing the fluid denaturation and annealing temperatures, respectively. These fluid temperatures were found at the center midpoint of each 180° bend at the top (denaturing) and bottom (annealing) of the channel. At low flow rates, it is clear this device is able to achieve the fluid temperatures required for PCR, for the heater temperatures applied. Significant temperature drop on the left and right sides of the device occurs due to end effects, which account for the heat transfer around the device, and arising from the assumption that the sides are completely insulated. It is clear that end effects dramatically affect the established temperature gradient. To reduce this effect, a longer entrance length could be incorporated into the design or the fluid could be given a higher inlet temperature. However, since both reactions reach the desired temperature, these methods are not necessary.

3.2 2D, 3D Comparison

With the 2D model producing results suggesting the device is capable of achieving the required denaturation and annealing temperature, the next step is to determine if the model is an accurate representation of the 3D device. To reduce the computational resources required to solve a large simulation, the center layer of the device with only 5-cycles is simulated in 3D. These results are compared to a 2D device simulation with the identical 5-cycle geometry. The 2D results presented in the previous section can also be compared. Ideally, all three simulations will agree with reasonable accuracy and the 2D simulation can be used for further analysis.

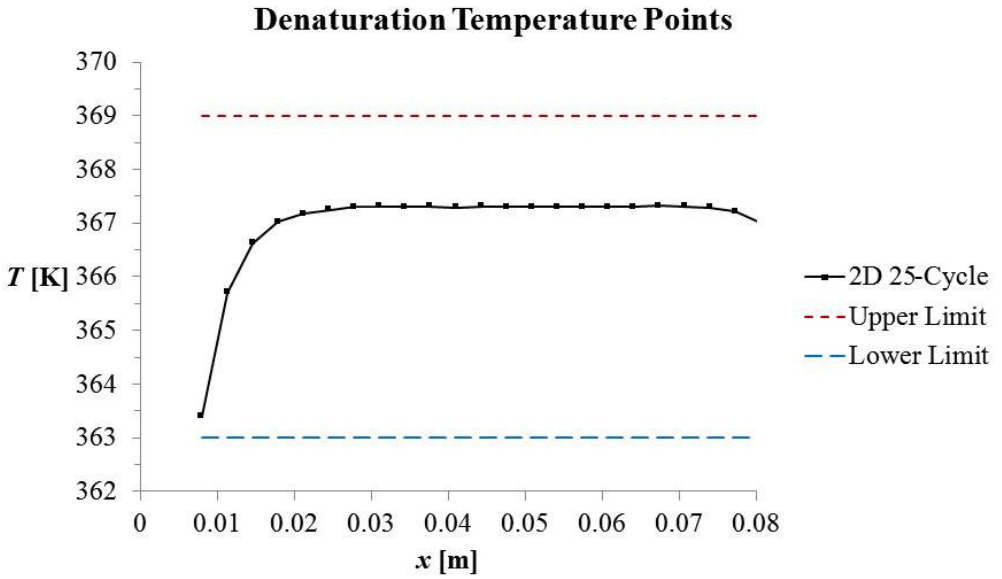

Figure 3.2: Denaturation temperature results from the 2D 25-cycle channel. The temperatures are measured in the center of the channel at each 180° bend nearest the hotter boundary condition. The acceptable temperature range for denaturation is represented by the dashed lines.

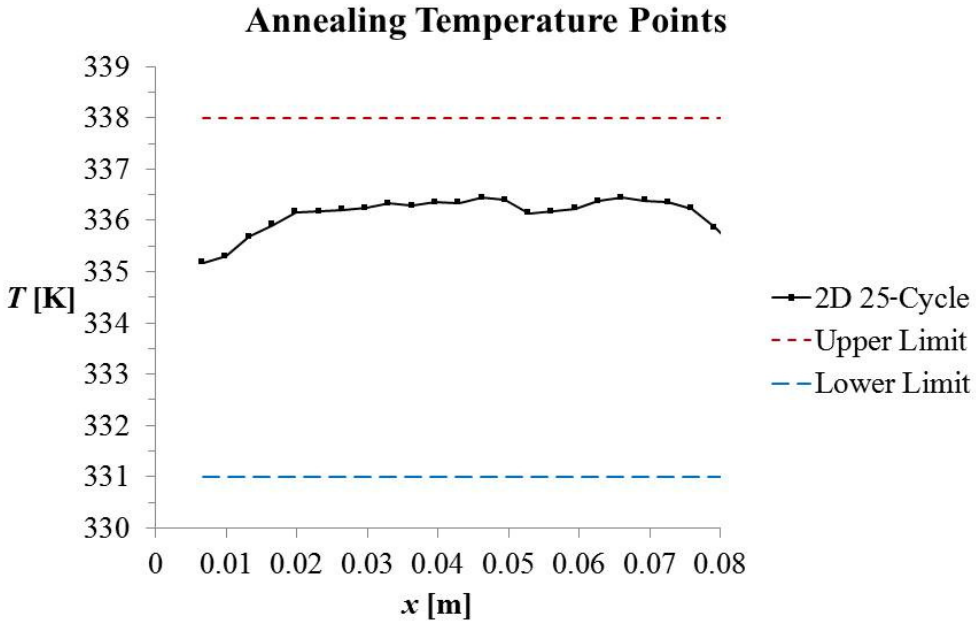

Figure 3.3: Annealing temperature results from the 2D 25-cycle channel. The temperatures are measured in the center of the channel at each 180° bend nearest the cooler boundary condition. The allowable range for annealing is represented by the dashed lines.

3.2.1 Boundary Conditions

The only difference when applying boundary conditions in 2D and 3D is that an area is defined in the 3D model as opposed to a boundary line in 2D. The same temperature and velocity boundary conditions are applied to the 2D and 3D 5-cycle models as the 2D 25-cycle simulation shown in Figure 3.1. Similar to a 2D 25-cycle model, any surface not defined as isothermal in a 3D model is considered adiabatic. This assumption has greater implications in 3D since it implies the top and bottom of the device are also insulated. The effects of heat loss from the system are neglected in this simulation but are presented in Chapter 4. Both simulation boundary conditions are shown in Figure 3.4.

3.2.2 2D, 3D Result Comparison

Both 5-cycle simulations were solved and are compared to the 2D 25-cycle data in Figures 3.5 and 3.6, representing the denaturation and annealing fluid temperatures, respectively. It is clear that a 2D approximation is not a valid assumption for this 3D device, despite the shallow channel thickness feature. It is interesting, however, that although the data do not agree well, the trends are very similar in the 2D and 3D simulations. With the intention of observing trends and largely disregarding actual values, two design considerations are analyzed qualitatively in 2D. The first is the effect of heater proximity to the fluid channel and the second is the entrance length. Insight into both design aspects can be gained by observing trends. More accurate data for these conditions are presented in Section 3.4.

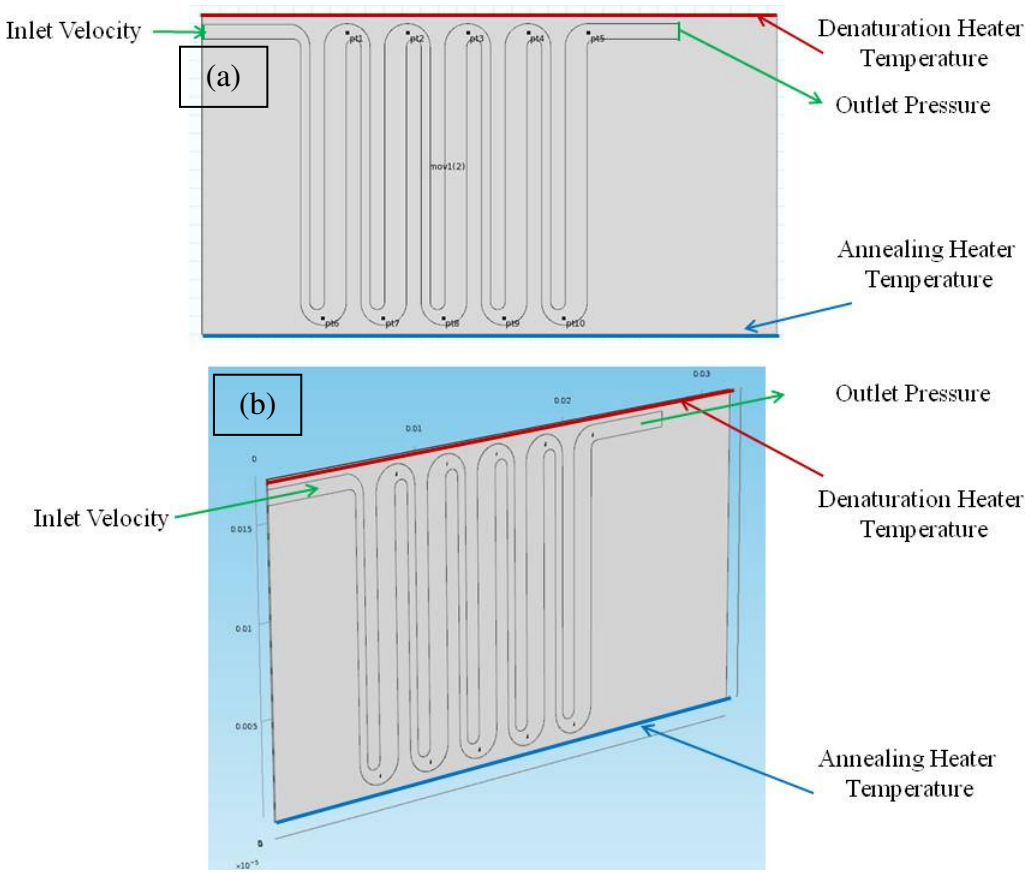

Figure 3.4: Boundary conditions for the 5-cycle channel in (a) 2D and (b) 3D. All areas not given an isothermal boundary condition are adiabatic.

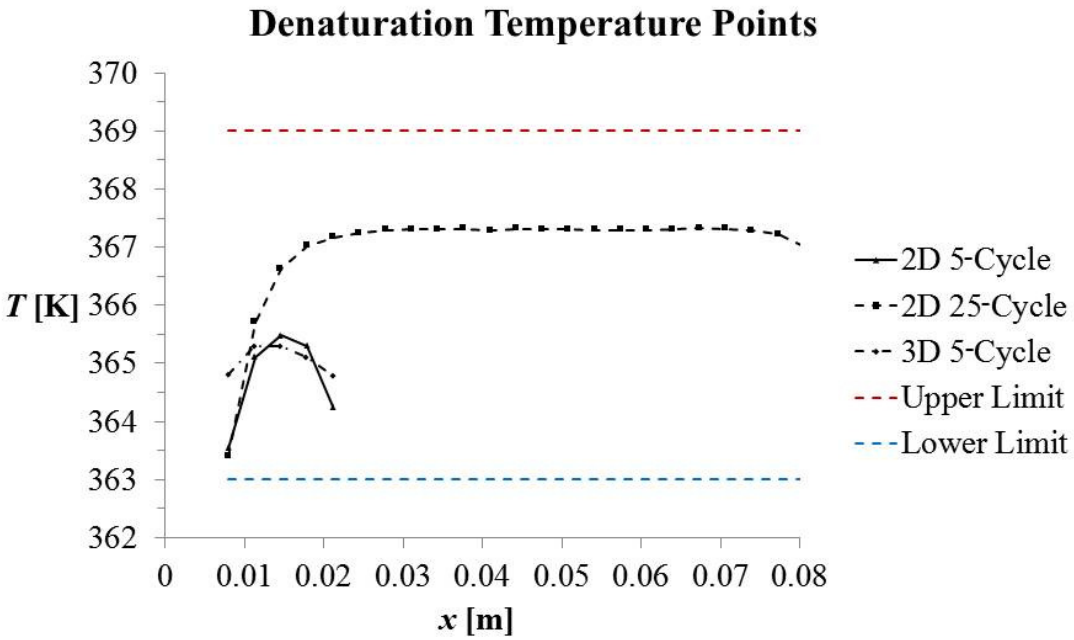

Figure 3.5: Denaturation fluid temperature comparison of the 5- and 25-cycle 2D simulations to the 3D 5-cycle simulation. The denaturation temperature range is represented by the dashed lines.

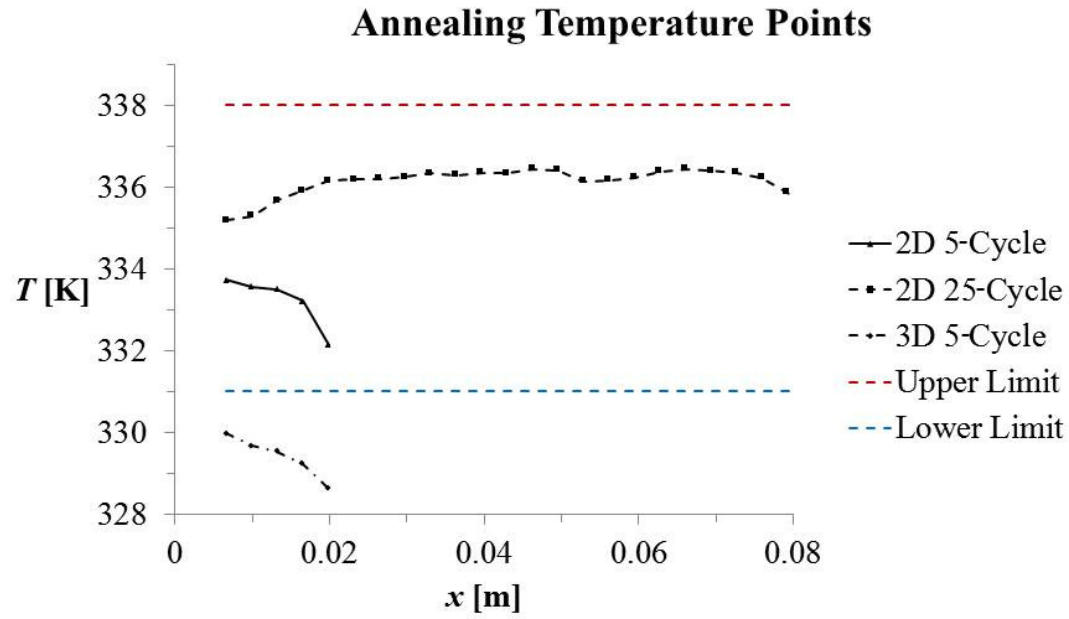

Figure 3.6: Annealing fluid temperature comparison of 5- and 25-cycle simulations to the 3D 5-cycle simulation. The dashed lines represent the upper and lower temperature limits for annealing.

3.3 Design Considerations

3.3.1 Heater Proximity

To observe the temperature gradient dependence on heater location, two simulations were completed; one with the heaters 3 mm from the edges of both the top and bottom fluid channels and the other with 0.5 mm separation. Each simulation was given the same boundary conditions shown in Figure 3.1 and the denaturation and annealing fluid temperatures are presented and compared in Figures 3.7 and 3.8, respectively.

From observation, the temperature profile is very dependent on the location of the heaters. When the heaters are 0.5 mm away from the fluid channel, each cycle reaches the desired reaction temperatures and an almost horizontal isothermal line is achieved along the device. However, when the heaters are positioned just 3 mm away from the fluid channel, the temperature profile is no longer constant and almost never achieves the required temperature ranges. From these data, it would be impossible to achieve PCR in a system with the heaters 3 mm from the channel and the same boundary conditions. These results will be taken into consideration during experimentation to ensure the heaters are positioned as close to the channel as physically possible. It is possible that the annealing and denaturation temperatures could be met in the system with the heaters 3 mm away from the fluid channel with the boundary conditions changed. However, recall that PC has a very low thermal conductivity, k = 0.20 W/m-K. It is difficult for heat to travel through this material. Therefore, placing the heaters as close to the fluid channel as possible allows the maximum amount of heat to go into the fluid as opposed to heating a volume of PC.

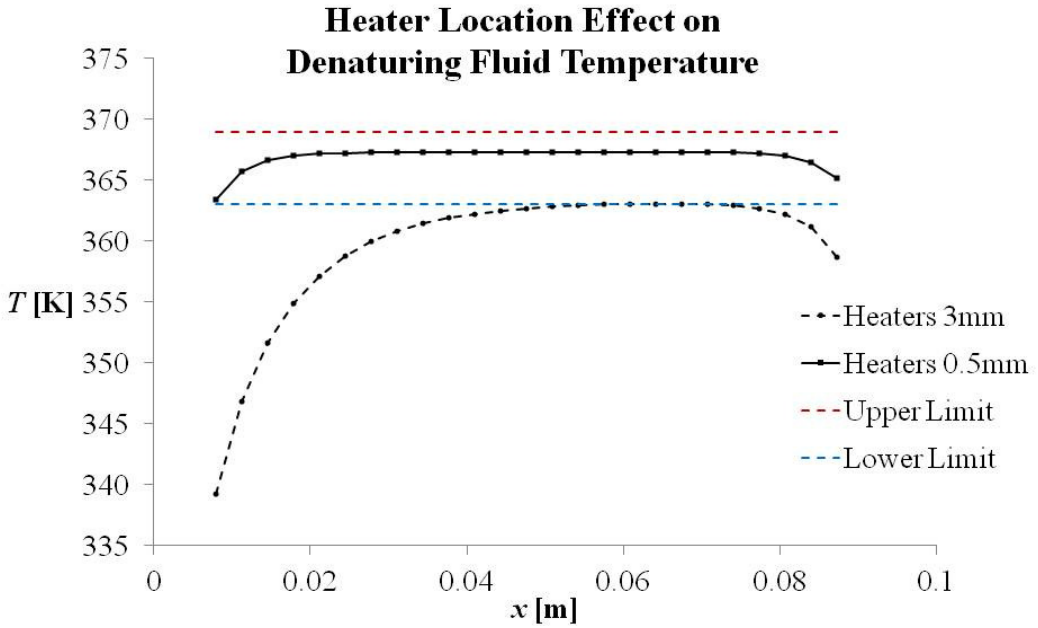

Figure 3.7: Midchannel fluid temperature in the denaturation region for two simulations with the heaters at different distances from the fluid channel.
The dashed lines signify the denaturation range.

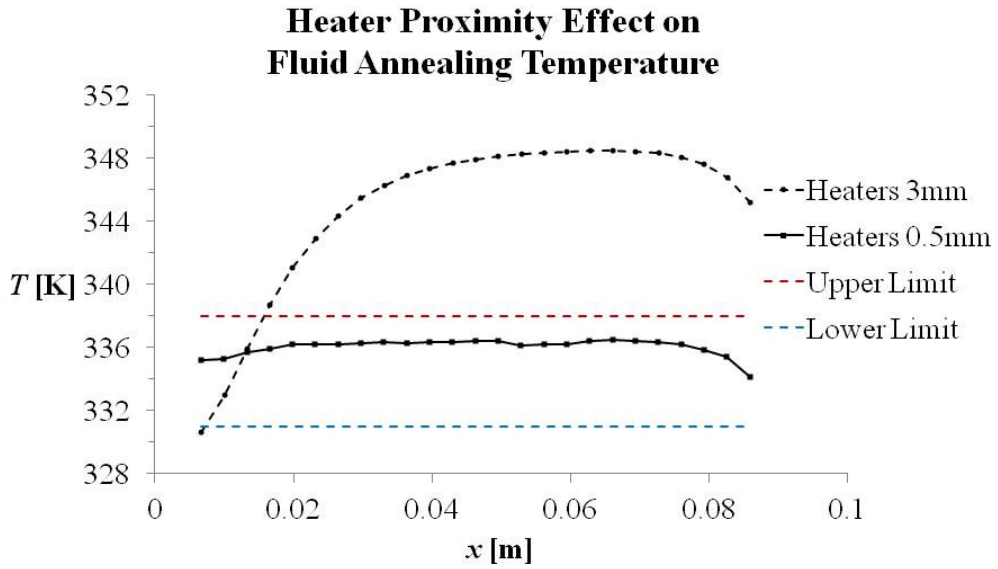

Figure 3.8: Midchannel fluid temperature data in the annealing region for simulations with the heaters placed at different distances from the fluid channel. The dashed lines signify the annealing range.

3.3.2 Entrance Length

The entrance length of the channel can also impact the fluid temperatures in each annealing and denaturing zone. The entrance length is the distance the PCR sample travels before entering the first denaturation bend. Ideally, the sample temperature just reaches the denaturation temperature before moving through the first bend. Three entrance lengths were examined, 5 mm, 10 mm and 15 mm, with the same boundary conditions as shown in Figure 3.1. The denaturation and annealing fluid temperature data are shown in Figures 3.9 and 3.10, respectively.

Despite the variety of entrance lengths, all resultant temperature profiles are within the required reaction temperature limits. It is clear the first several denaturation cycles are greatly impacted by the entrance length and that the annealing temperature profile is not affected as dramatically. These results suggest the entrance length must be optimized for a given set of temperatures and flow rates. Based on these results, further simulations use a 5mm entrance length to reduce the simulation total mesh size but 10mm is used for experimentation due to the linear nature of the results.

3.3.3 Discussion

It has been shown that a 2D simulation for this microfluidic device is not an appropriate approximation for the 3D system; however, both simulations produced similar trends. From qualitative observation, it has been shown that more uniform annealing/denaturing temperatures are created when the heaters are placed very close to the fluid channel and that the entrance length must be designed for specific flow rate and temperature conditions.

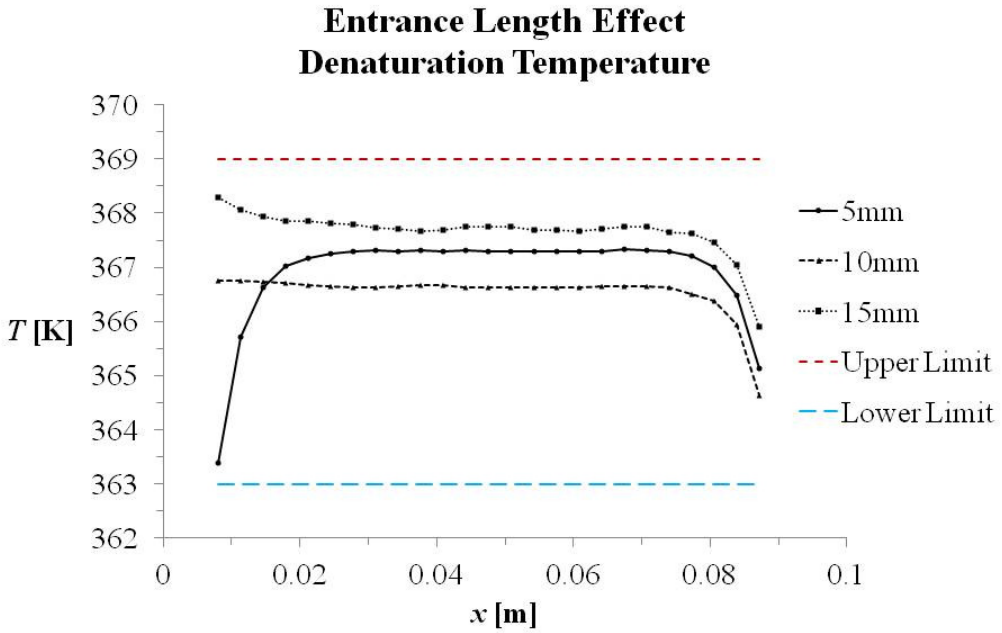

Figure 3.9: Midchannel fluid temperature data at the middle of the denaturation bends for a variety of entrance lengths. The dashed lines represent the denaturation temperature range.

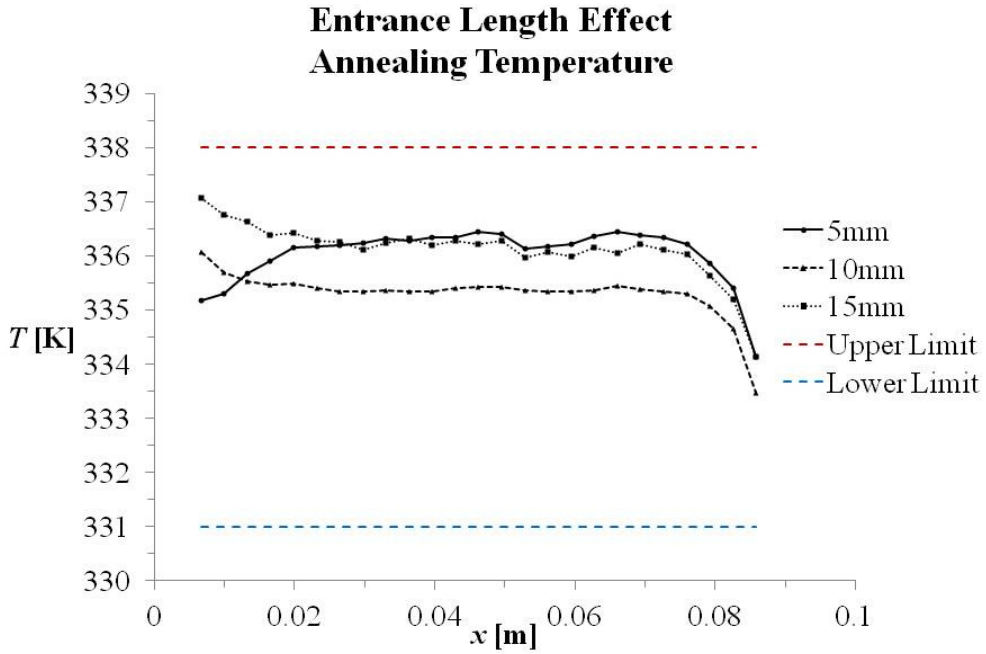

Figure 3.10: Temperature from points in the annealing turn for a variety of entrance lengths. The dashed lines represent the annealing temperature range.

3.4 3D 25-cycle Simulation Methods

Although information is gained by observing the trends exhibited in the 2D model, it is imperative to know the actual fluid temperatures through the channel to ensure the entire sample is reaching the reaction temperatures during each cycle. A simplified 3D device with 25-cycles is modeled in COMSOL.

3.4.1 Assumptions and Simplifications

The geometry used to represent the device must be simplified in order to allow a refined mesh that accurately simulates the physics of the device while reducing the number of mesh elements, enabling the simulation to be solved with available computer hardware. Thus, the three-layer device with attached heaters is reduced to just the center PC layer and water channel. Heat transfer simulations are solved to justify each simplification.

In the first simplification, the heaters and the device area on which the heaters rest both above and below the fluid channel are removed. The heaters can easily be removed with the assumption that the interface between the heater and device is isothermal. Including the heater in the simulation is not necessary and only adds additional mesh elements. In the same way, assuming there is negligible temperature variation through a single layer of 0.00011 m thick PC, the bulk material above and below the device can be eliminated from the simulation. The model is now simplified to a smaller three-layer device as depicted in Figure 3.11.

In the second simplification, the top and bottom PC layers are removed and only the center layer with the fluid channel is analyzed, as shown in Figure 3.12. A heat

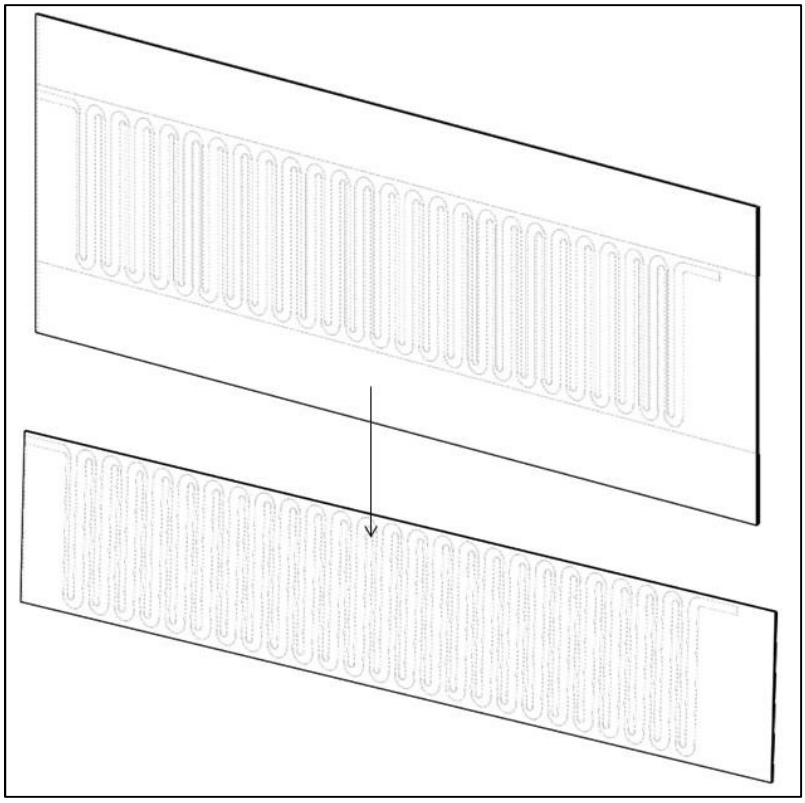

Figure 3.11: Schematic showing simplification accomplished by removing the heaters and device area where the heaters interface.

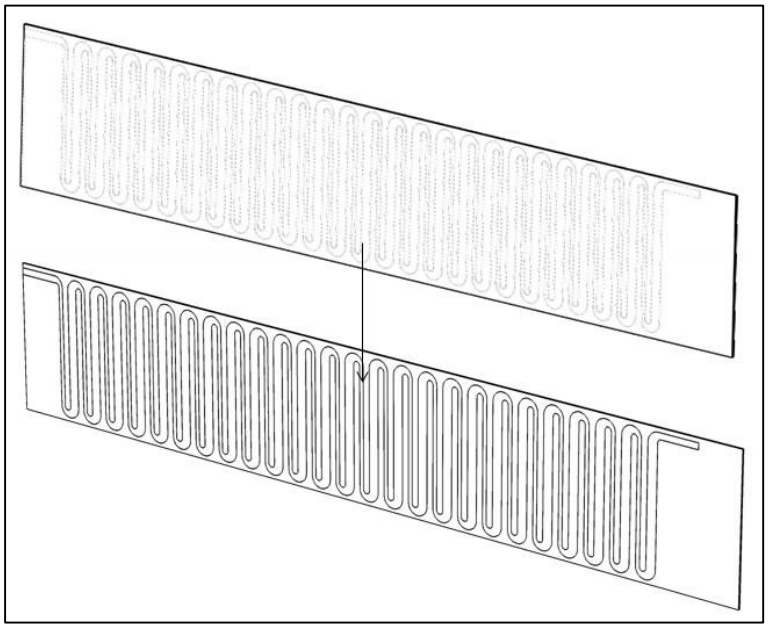

Figure 3.12: Schematic showing the simplification of removing the outer layers of the device for purposes of reducing overall mesh size.

transfer analysis is completed assuming the fluid is present but not flowing. To demonstrate that the top and bottom layers are not important to the solution, the temperature profiles along the device on both sides of the bottom layer are plotted in Figure 3.13.

As shown in Figure 3.13, the bottom-center interface temperature is only about one degree less than the defined heater temperature. The temperature discrepancy near the channel entrance is due to the propagation of the room temperature (20°C) defined inlet fluid temperature. This entrance effect can be ignored if the entrance length is greater than 5 mm, because the low temperature consequence is damped out after this distance. Since the temperature difference between the two locations is small (less than 0.01 K), this difference can be considered negligible. By neglecting these minor temperature fluctuations and reducing the heater temperature slightly during the experiments, it can be assumed that a one-layer device, shown in Figure 3.14, is an appropriate approximation for this three-layer PCR device.

3.4.2 Boundary Conditions

The one-layer 3D model requires the heater temperatures, and fluid inlet temperature and mean velocity to be defined. The inlet fluid temperature is defined as room temperature, 293.15 K, and the inlet mean flow velocity is varied to represent a volumetric flow rate between 0.1 mL/hr and 1 mL/hr. Note that both the temperature and velocity were assumed to have uniform values in the entrance cross-section. The conversion between flow velocity (V) and flow rate ($\dot{V}$) depends on the cross-sectional area (A) of the channel and is defined in Eq. 3.2.

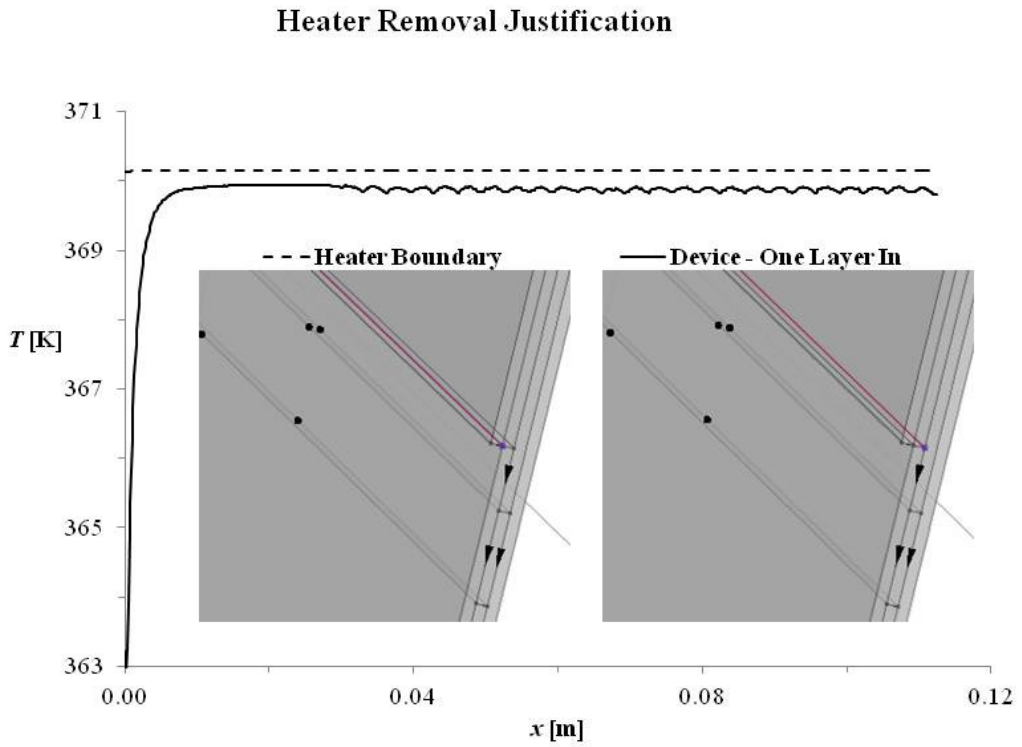

Figure 3.13: Temperature profile on the outside of the bottom layer compared to the temperature profile on the other side of the bottom layer, which interfaces with the fluid channel. Line of interest is highlighted in red.

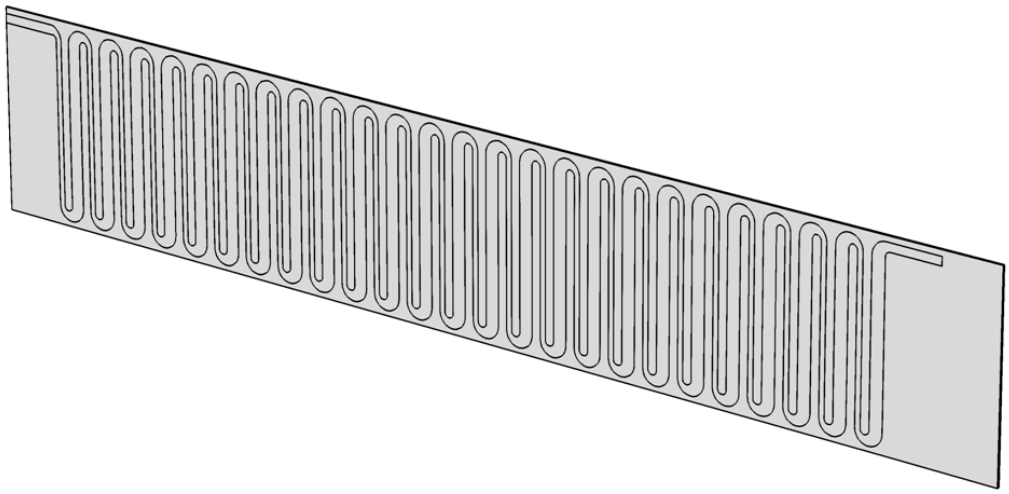

Figure 3.14: SolidWorks model of the simplified 3D, one-layer channel used to explore end effects and ensure PCR reaction temperatures can be met in a PC device.

$$V = \frac{\dot{V}}{A} \qquad [3.2]$$

Isothermal boundary conditions (representing the heater temperature) are applied to the top and bottom areas perpendicular to the flow plane. These isothermal temperatures are adjusted with flow rate. The front, back and sides are all considered to be adiabatic. These boundary conditions are summarized in Figure 3.15. Chapter 4 will discuss a separate simulation which analyzes the effects of convection and radiation from the top surface. Despite heat being input into the system from the top and bottom, the model satisfies the conservation of energy principle because the energy entering the system is able to leave with the fluid.

3.4.3 Mesh Refinement and Convergence Criteria

A driving force for simplifying the device geometry was to find a balance between a refined mesh and the capabilities of available computing resources. The finest mesh in the system is required in the fluid channel to accurately produce a realistic flow field. By requiring that at least three nodes are located across the fluid channel height, the

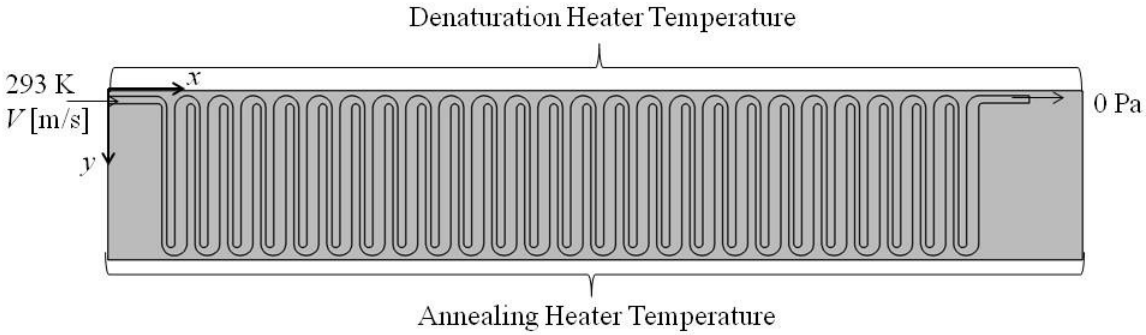

Figure 3.15: General boundary conditions for the 3D 25-cycle simulation. Although not shown, this model has a depth of 0.00011m.

simulation is solved with 4.4 million mesh elements. To ensure this mesh produced accurate results, a simulation with 5.4 million mesh elements was completed and the maximum velocity varied less than .02%. Since Section 3.1.3 discussed that errors less than 2% can be considered fully converged for the presented simulations, the smaller of these two mesh sizes was deemed sufficient for simulation accuracy. The same convergence criterion was used for this simulation as the 2D model.

3.4.4 Results: Material and Design Validation

One of the main purposes of this simulation is to validate that polycarbonate is a legitimate material for CF-PCR, and determine appropriate heater settings for a variety of flow rates. Temperature within the fluid channel is analyzed at points defined in the center of each 180° serpentine bend. The nodes where the temperature is measured are shown in Figure 3.16. Maintaining constant flow rate, the heater temperatures were adjusted until the temperatures of the hot side measurement points were within the denaturation temperature range of 90°C to 96°C and the measurement points on the colder side had temperatures within the annealing temperature range of 58°C to 65°C.

With the denaturation and annealing heater temperatures defined as the values in Table 3.1 for a given flow rate, the fluid was able to achieve the temperatures presented

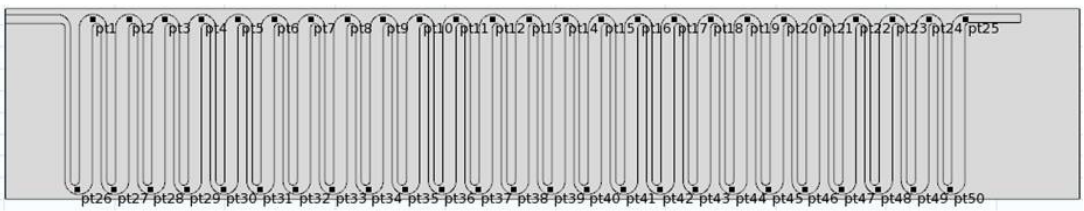

Figure 3.16: Geometry of channel with defined nodes to measure temperature

Table 3.1: Temperature boundary conditions used for the 3D, 25-cycle device as the flow rate is varied.

Flow Rate [mL/hr]	**Heater Temperatures [K]**	
	Denaturation	**Annealing**
0.1	370	330
0.25	376	330
0.5	390	319
1	405	305

in Figures 3.17 and 3.18 for denaturation and annealing, respectively. An upper and lower limit for each reaction is given to show if the reaction could be deemed successful.

For flow rates below 0.5 mL/hr, both reaction temperatures are well within the appropriate ranges and PCR could confidently be completed. At a flow rate of 0.5 mL/hr, almost all the reaction nodes meet the desired temperatures with the exception of the first and last point on the denaturation side. These temperatures could be brought up to the reaction temperature by either heating the sample before it enters the channel or adjusting the heater settings further. However, as the flow rate is increased to 1 mL/hr, it is clear that the reaction temperatures are not met. Despite a 100°C difference between the heater temperatures, the fluid does not have adequate time to adjust to the reaction temperatures. It is possible these temperatures could be achieved by including a fin array on the annealing side to encourage heat flow away from the system or if the channel width was increased to allow for a larger residence time. This model suggests the device could achieve satisfactory PCR with a flow rate at or below 0.5 mL/hr.

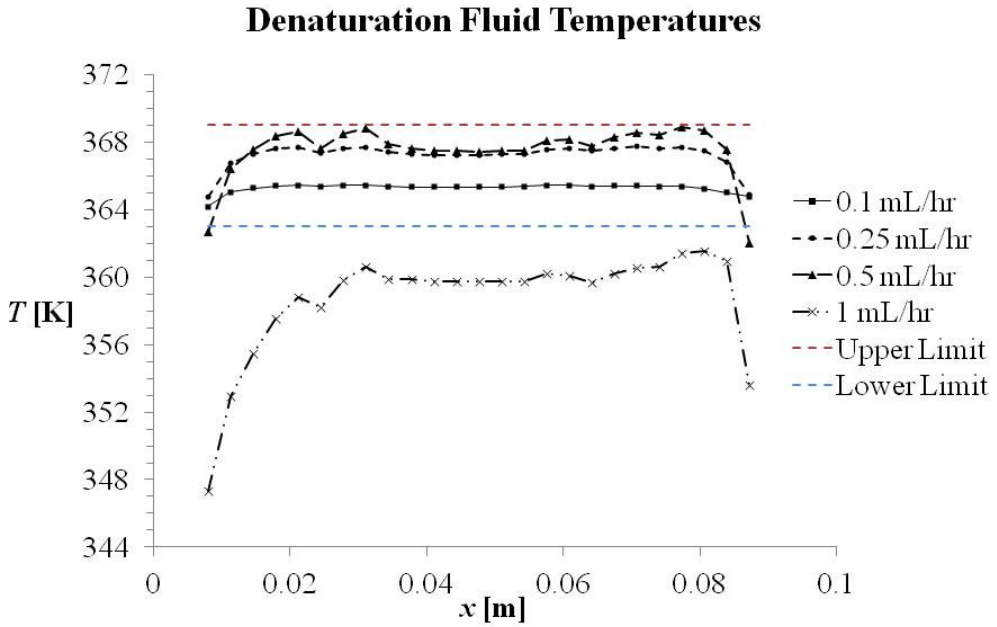

Figure 3.17: The fluid temperature within the channel for varying flow rates during denaturation.

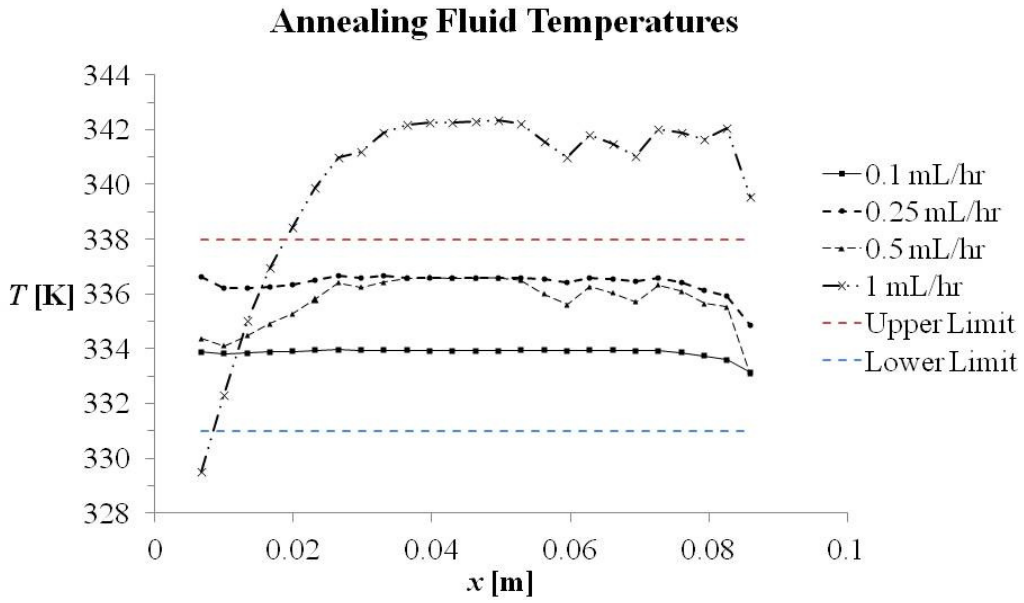

Figure 3.18: The temperature profile for the annealing phase for four different flow rates.

3.5 Flow Plane Discussion

From these simulation results, it can be concluded that, with the correct boundary conditions and an appropriate flow rate, PCR can be achieved in a PC device with the given geometry. As discussed in Chapter 2, with a flow rate of 1 mL/hr, a cycle time of 15 seconds is expected, resulting in a total reaction time of 6.7 minutes. However, the data presented herein suggest that this flow rate will not allow the PCR reactants to reach the required temperatures. If a flow rate of 0.5 mL/hr is used, the total reaction time becomes 13.3 minutes. Many other microfluidic devices have been shown to complete the entire PCR reaction in times less than this. To decrease this reaction time, the flow rate must be increased. To do this, a more appropriate representation of the system must be modeled.

Thus far, all the presented simulations assume that all the heat generated by the heaters is going directly into the device. In reality, heat will be lost to the environment by radiation and convection, which will have a large impact on system performance. These forms of heat loss may also have the potential to aid in accomplishing PCR by removing heat in the high flow rate scenarios. An analysis of the heat lost must be completed to understand how the device will perform in a lab setting. It is expected that the temperature boundary conditions will also need to be adjusted.

CHAPTER 4

NORMAL TO FLOW COMPUTATIONAL METHODS AND PROCEDURES

Although the simplified one-layer device presented in Chapter 3 has its purpose, it is important to analyze the system with more realistic boundary conditions and consider the heat transfer normal to the flow plane. Examining how much heat is lost from the top of the device is important in understanding how these losses to the surroundings affect the imposed fluid and solid temperature gradients at a variety of flow rates. To comprehensively study these effects, the heat loss from the device was analyzed along with several different insulating scenarios to determine which insulation scheme is most efficient. The four insulating cases are: glass directly on top of the device, and an insulating chamber encased by glass filled with air, argon and a vacuum. One-dimensional calculations were first completed to determine which insulating method is most effective. A two-dimensional simulation was solved to observe how parameters affected system performance. Then, the best scenario was simulated in three dimensions for one cycle of the device with periodic boundary conditions. This 3D model was applied to analyze the heat lost from the system, to determine ideal heater set-point temperatures for a few flow rates and to the correlate fluid and device temperatures.

4.1 1D Calculations

Each insulating scenario is analyzed with a 1D thermal resistance model. The bottom of the device is assumed to be completely insulated at a specified temperature of 373K; therefore, all the heat travels out through the top of the device. By defining this temperature at a high value, the worst-case scenario for heat loss is represented. Also, the device is assumed to be a single layer with a thickness of .45mm and no fluid is present. Any thermal contact resistance between the PC and the glass is neglected.

4.1.1 Scenario 1: Device Only, No Insulation

To provide a basis for comparison, the device is first analyzed without any insulation. This system involves conduction through the PC layer, and convection and radiation from the top of the device to the surroundings. The temperature at surface 1 is defined. The thermal resistance model is shown in Figure 4.1. The total heat lost from this simple system is found from Eq 4.1.

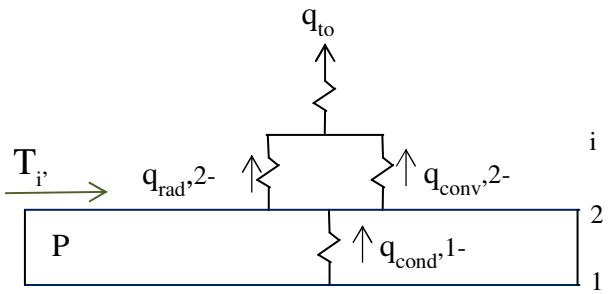

Figure 4.1: Thermal resistance schematic of polycarbonate without any additional insulation. This model is completed to show how important insulation is to the system.

$$q_{tot} = q_{cond,1-2} = q_{conv,2-i} + q_{rad,2-i} \quad [4.1]$$

Conduction between any two surfaces is defined in Eq 4.2,

$$q_{cond} = \frac{T_a - T_b}{\frac{L}{kA}} \quad [4.2]$$

where k is the thermal conductivity of PC, and A is the area of the chip. Convection off the top surface is calculated using Eq 4.3.

$$q_{conv} = \frac{T_a - T_b}{\frac{1}{hA}} \quad [4.3]$$

T_a is the temperature on the surface where the heat is leaving and T_b is the temperature where the heat is going to. The convective heat transfer coefficient is defined as h.

The last heat transfer effect to account for is radiation from the top surface, which can be calculated from Eq 4.4.

$$q_{rad,surface-surroundings} = \frac{\sigma(T_{surf}^4 - T_i^4)}{\frac{1}{A\,\varepsilon_{PC}}} \quad [4.4]$$

The Stefan-Boltzmann constant, σ, is always defined as 5.67E-8 W/m^{2}K^4, the glass surface temperature is defined as $T_{surf,}$ T_i is the surrounding temperature and ε_{glass} is the emissivity of glass which was assumed to be approximately 0.9.

4.1.2 Scenario 2: Glass Only

The simplest method for reducing convection effects is to place a glass substrate on top of the working device to provide a layer of insulation. The thermal resistance model is shown in Figure 4.2. The heat lost from this system is calculated from a thermal model shown in Eq. 4.5. The thickness of the glass piece can be varied during analysis; however, this information is not presented since a standard microscope slide is used during the experiments.

$$q_{tot} = q_{cond,1-2} = q_{cond,2-3} = q_{conv,3-i} + q_{rad,3-i} \quad [4.5]$$

4.1.3 Scenarios 3 and 4: Air and Argon Gap

By including a gap between the PC and glass layers, convection and radiation thermal resistances are added. The thermal resistance model is shown in Figure 4.3. The air and argon models are shown together because both scenarios share the same

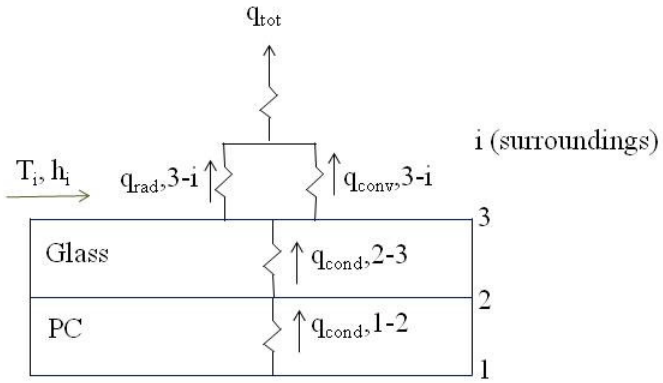

Figure 4.2: Thermal resistance model of system with glass on top of PC. The glass adds an additional conduction term to the model.

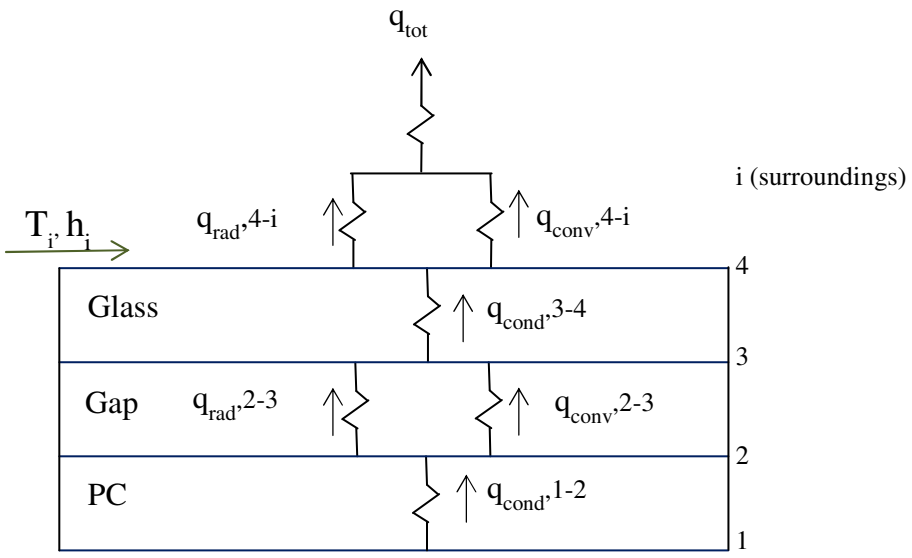

Figure 4.3: Thermal resistance model for an insulation system with a gap. This gap was analyzed with both air and argon inside. For the right conditions, convection occurs in the gap

equations and only differ by gas properties. Convection effects can be observed in gas enclosures if the Rayleigh number (*Ra*) is between approximately 1708 and $5x10^4$. Below *Ra* = 1708, viscous forces dominate and no advection occurs; however, the gas will still represent a conduction resistance. Above 5E4, turbulent flow occurs and the flow is not easy to predict. The total heat loss from this system is found in Eq 4.6.

$$q_{tot} = q_{cond,1-2} = q_{conv,2-3} + q_{rad,2-3} = q_{cond,3-4} = q_{conv,4-i} + q_{rad,4-i} \quad [4.6]$$

The view factor is an important parameter when analyzing radiation between two surfaces and is defined as the fraction of the radiation leaving one surface that is intercepted by another [35]. For a parallel plate, the view factor is assumed to be one and the radiation between two surfaces can be reduced to Eq 4.7. The emissivity values used for this calculation were based on average values for the material. The emissivity of PC is

assumed to be 0.88 and that of glass is 0.90. The convection within the enclosure is found from Eq 4.8.

$$q_{rad,2-3} = \frac{A_s \sigma (T_2^4 - T_3^4)}{\frac{1}{\varepsilon_{pc}} + \frac{1}{\varepsilon_{glass}} - 1} \quad [4.7]$$

$$q_{conv,2-3} = \frac{T_2 - T_3}{\frac{1}{h_{Nu} A}} \quad [4.8]$$

The convection coefficient h_{Nu} is calculated from the Rayleigh number- dependent Nusselt number correlation, as discussed in Chapter 2. An assumption made during the h_{Nu} calculation for argon is that the Nusselt correlation, which was derived for air, may also be used for argon. The derivation of this correlation has a strong dependence on the Prandtl number. Since air and argon have Prandtl numbers of 0.7 and 0.6687 at 20°C and 1 atm, respectively, this assumption is deemed appropriate. Convection may not present in the enclosure when the *Ra* is less than 1708, but conduction is. This can be represented by Eq 4.8 using *Nu* = 1.0.

4.1.4 Scenario 5: Vacuum Gap

By evacuating the chamber and creating a vacuum, both convection and conduction in the chamber are eliminated. The thermal resistance model is shown in Figure 4.4. Total heat transfer is reduced, with only radiation transferring heat across the gap. The total heat lost from the system is found in Eq 4.9.

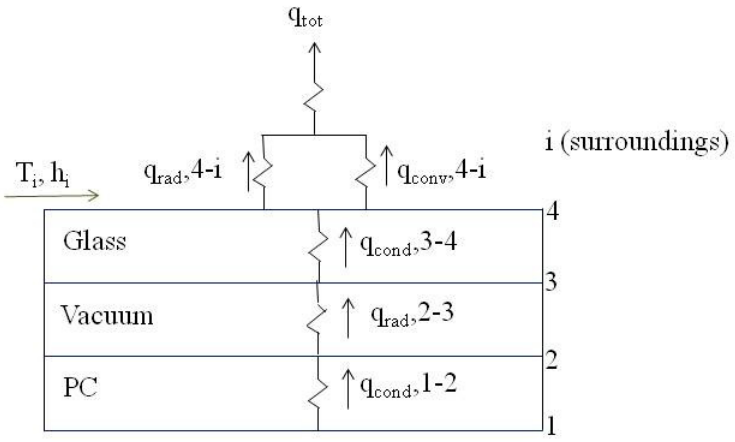

Figure 4.4: Thermal resistance model for an insulation scenario where there is a vacuum gap between the PC device and glass. The only heat transfer occurring in this gap is by radiation.

$$q_{tot} = q_{cond,1-2} = q_{rad,2-3} = q_{cond,3-4} = q_{conv,4-i} + q_{rad,4-i} \quad [4.9]$$

This is expected to be the most efficient insulating scenario due to the removal of the heat transfer medium in the gap. It is clear from Figure 4.5 that including any kind of chamber reduces the heat loss significantly. To quantify this observation, Table 4.1 summarizes the percent increase in performance from the previous case, which will show the case that has the most significant improvement.

4.1.5 1D Results and Comparisons

The heat loss from the top of the glass surface is compared for each scenario for varying heat transfer coefficient on the top surface in Figure 4.5 assuming a glass thickness of 1.5mm and a gap thickness of 6mm.

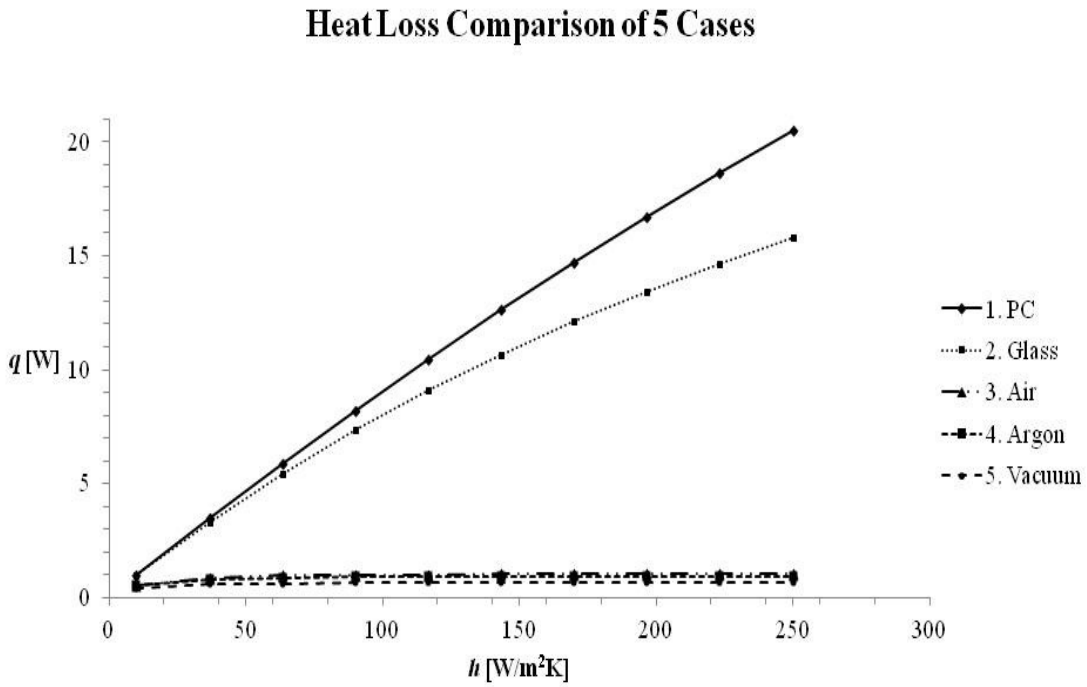

Figure 4.5: Heat loss for the five insulation scenarios as a function of the convection coefficient.

The largest percentage increase in system performance, defined as low heat transfer to the surroundings, is noticed between Scenario 2 (glass only) and Scenario 3 (air chamber), as expected. Table 4.1 also shows that the addition of a chamber makes a larger difference in high convection environments. From Figure 4.6, which zooms in on the three chamber cases, the vacuum chamber scenario is most effective at reducing heat loss, followed by the argon gap, then the air gap.

Although the vacuum gap is the most effective, it is the hardest to fabricate and maintain. One large advantage of manufacturing a disposable device is that initial cost is relatively low. By adding a vacuum chamber, the associated cost would increase significantly, eliminating the initial low manufacturing cost advantage. The same

Table 4.1. Performance percentage increase between each insulation scenario.

Case	Description	q [W], h = 10 W/m^2-K, T_∞ = 298 K	% Increase from Previous Case	q [W], h = 250 W/m^2-K, T_∞ = 298 K	% Increase from Previous Case
1	PC Only	0.9687	-	20.53	-
2	Glass Only	0.9552	1.394	15.78	23.137
3	Air Chamber	0.5401	**43.457**	1.052	93.333
4	Argon Chamber	0.5124	5.129	0.9364	10.989
5	Vacuum Chamber	0.4282	16.432	0.6558	29.966

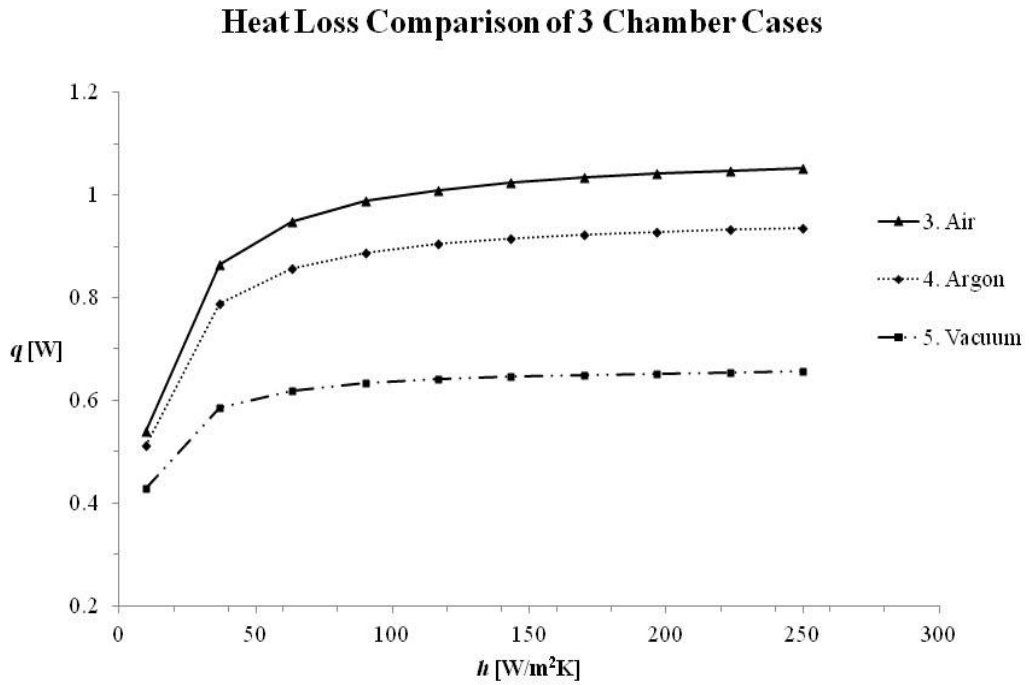

Figure 4.6: Same information as Figure 4.5, but with the three most efficient insulation scenarios.

problem arises with the next most efficient scenario, the Argon-filled chamber. Sealing and gas delivery would be complicated and expensive. Therefore, an air-filled gap is deemed to be the most effective both in terms of reducing heat loss and cost.

A closer analysis of the heat transfer within the enclosure will determine if one type of heat transfer, conduction/convection or radiation is dominant. If one is significantly larger than the other, then the other could be assumed to be negligible. It is found that the radiation in the enclosure accounts for approximately half of the heat being transferred in the chamber and therefore must be kept in the model.

More simulations were completed by varying the air gap thickness, convection effects and ambient temperature. The following trends were observed. As the gap thickness increases, the heat loss decreases despite the increasing chamber convection effects; as the convection effects on top of the device increase, the heat loss also increases; as the surrounding temperature increases and approaches the device temperature, the heat loss decreases. From this information, the ideal design for the CF-PCR insulation is a large air gap between the device and glass slide and the ideal environmental effects should include low convective effects and warm surrounding temperature.

4.2 2D Simulation Methods and Procedures

4.2.1 Simulation Validation

The device is now represented in two dimensions to observe the heat transfer out of the flow plane, as shown in Figure 4.7. The fluid channel is defined but a no- flow condition is assumed. The entire device is considered to be insulated except the top

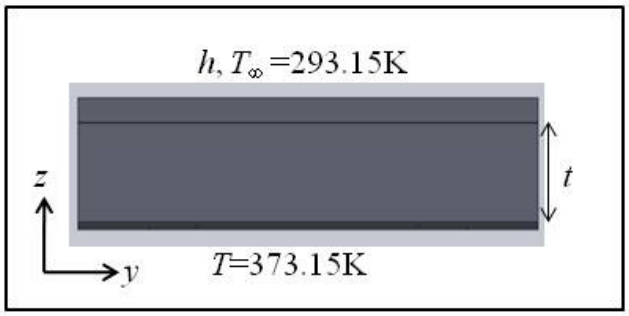

Figure 4.7: Boundary conditions for the 1D validation. All surfaces not defined with a temperature, or experience convection or radiation, are considered insulated.

surface which experiences convection and radiation to the surroundings. The 1D calculations are used to validate this simplified 2D model and ensure the simulation is producing acceptable results. The entire bottom surface is assumed to have a temperature of 373K. This low temperature will create a worst-case scenario and match the 1D calculation inputs.

Since this two-dimensional simulation was given boundary conditions to replicate a 1D system, the entire top boundary resulted in a uniform temperature. This temperature was compared to the 1D simulation results for the same convection and air gap thicknesses. The results were within 0.5% of each other, validating the two-dimensional simulation was solving the equations correctly.

4.2.2 Two-Dimensional Simulation Boundary Conditions

Contrary to the bottom surface being held at one temperature, as observed in the one-dimensional analysis, the bottom layer has a temperature gradient, which will impact the system performance. With the 2D model validated, more realistic boundary conditions are imposed. The heater areas are given a defined temperature and the fluid is

again defined but is not given a velocity. These boundary conditions are shown in Figure 4.8. This simulation represents the system with water in the channel, but with no flow.

The temperature gradient on the top of the glass surface is calculated and the heat loss can then be determined by Fourier's Law. The temperature profile is found on the surface and at a distance 0.00015m into the surface. The heat loss is calculated from Eq 4.11 where ΔT is the change in temperature between the surface and slightly below the surface and Δz is 0.00015m.

$$q'' \approx \frac{\Delta T}{\Delta z} \qquad [4.11]$$

In order to completely analyze the convection effects, the simulation is solved with a convective heat transfer coefficient, h, of 2, 10, 25, 100 and 250 W/m^2-K. Recall natural convection with air experiences an h between 2 and 25 W/m^{2}K while forced convection occurs from 25 to 250 W/m^2-K. [35] In a lab setting, an h value between 10

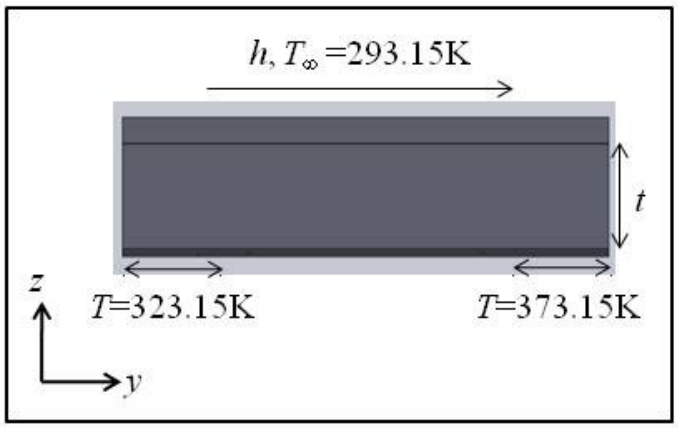

Figure 4.8: Boundary conditions for the 2D heat transfer model of the system. No fluid motion considered.

and 20 is realistic; however, extremes are studied to examine the potential consequences of using this device in the field.

4.2.3 Mesh Refinement and Convergence Criteria

Since this particular simulation determines only the temperature field, the temperature along the glass surface is used for determining the effect of mesh size. A mesh with 143098 mesh elements is used to solve this problem and was compared with a mesh of 172081 mesh elements. An error of only .002% was found between the temperatures along the glass surface. Using the discussed assumption that 2% error is fully converged, the results presented can be assumed accurate.

The simulation is assumed to be completely solved when the solution at each node is changing less than 0.1% between consecutive iterations. If the simulation reaches 100 iterations without finding a solution, it is determined that the solution is not converging and an error message appears.

4.2.4 Results

The results from this simulation are presented in two forms. First is the case where a constant h value is defined while the air gap thickness is varied and the second is with the air gap thickness held constant and the h value varying. Plots for constant h values of 2, 10, 25, 100 and 250 W/m^2-K are presented in Figures 4.9-4.13. The 4mm air gap thickness results are presented in Figure 4.14 where the trends can be assumed similar for the other gap thicknesses. The temperature distribution along the x-direction of the glass edge was converted into heat loss by Fourier's law defined in Eq 4.11.

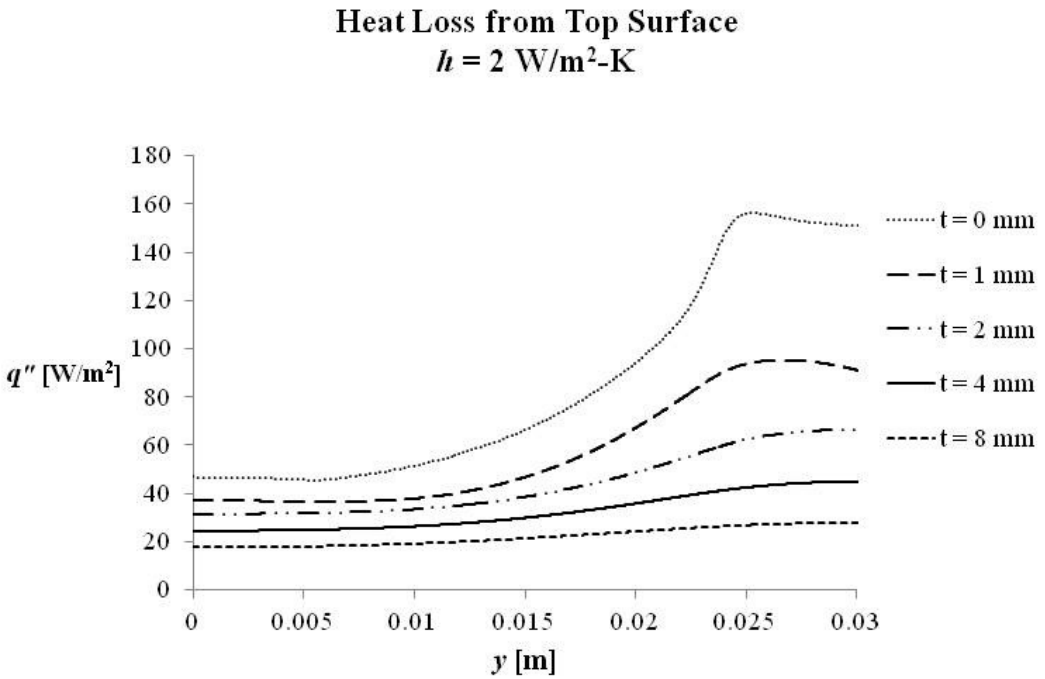

Figure 4.9: Heat loss from the top surface of the 2D device. The air gap thickness is varied from no gap to a gap of 8mm. Notice that as the thickness increases, the heat loss decreases.

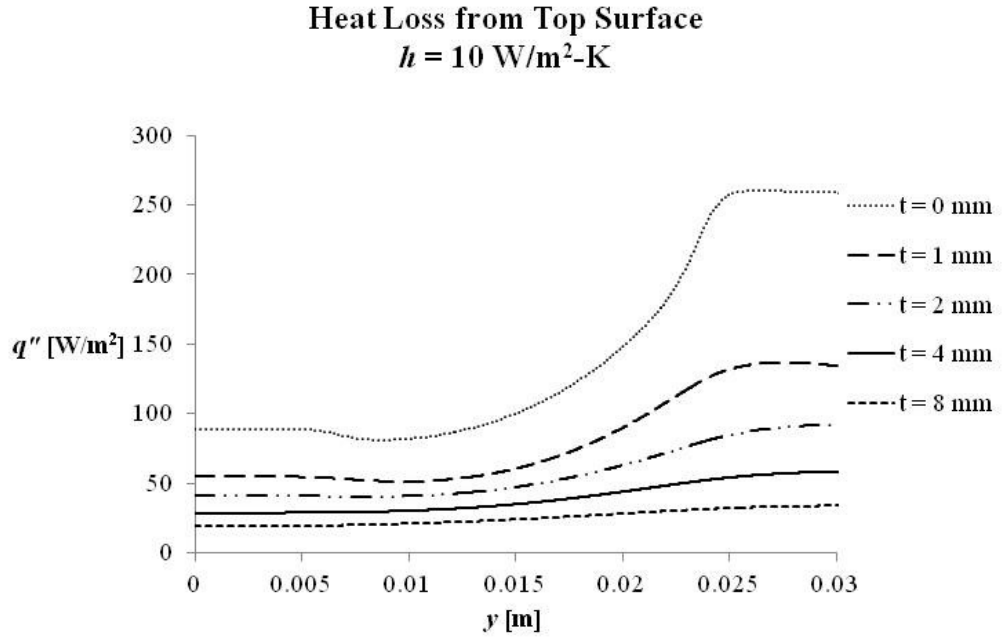

Figure 4.10: Heat loss from the top surface with varying air gap thicknesses. The convection effects are slightly higher here, causing the heat loss to be greater than with the lower convection coefficient.

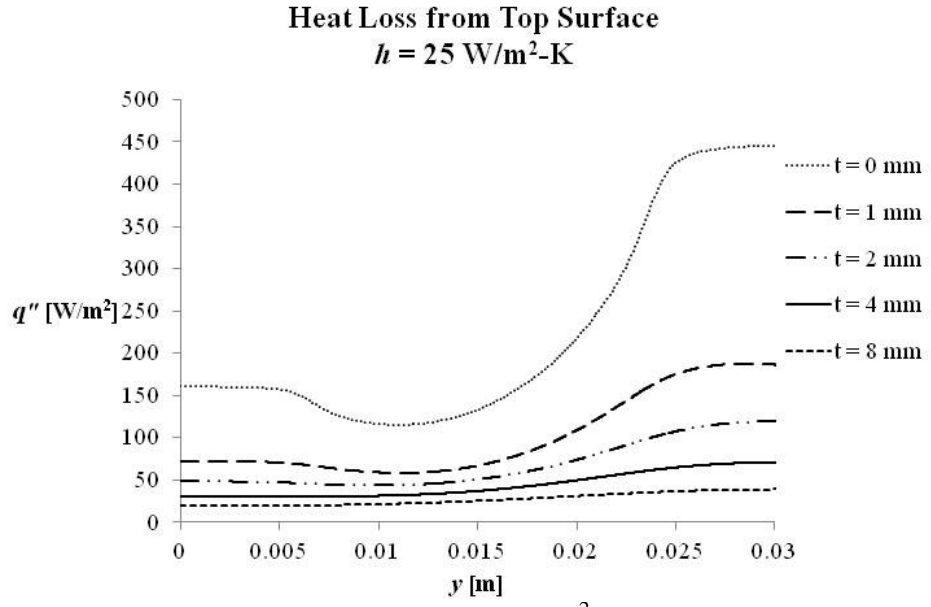

Figure 4.11: With a convection coefficient of 25 W/m^2-K, less heat is lost in the center of the devices with small or no air gap. This implies that the device temperature above the fluid channel is cooler than either heater temperature due to larger impact convection effects have on smaller air gaps.

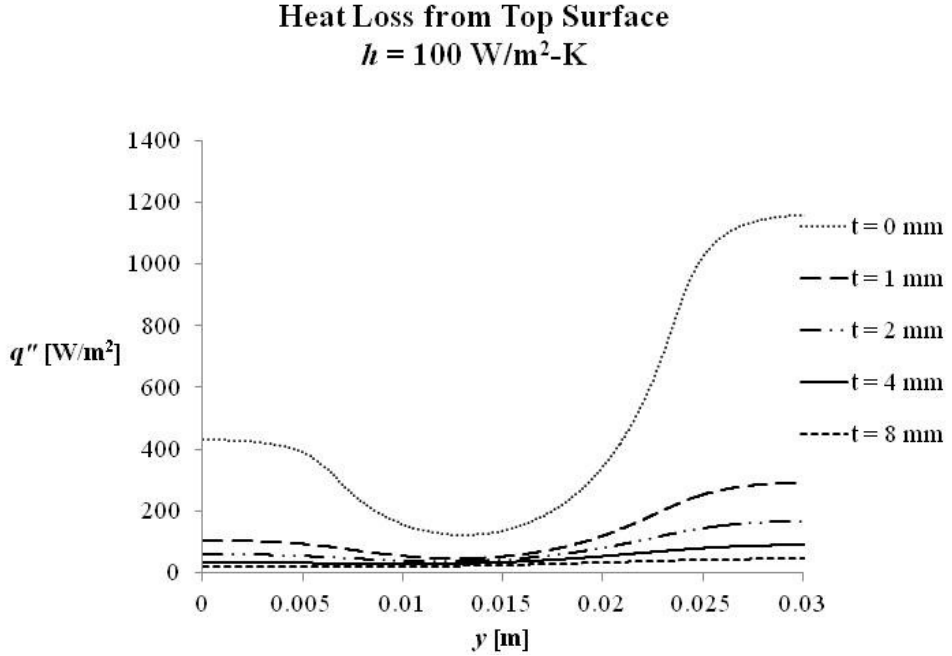

Figure 4.12: As the convection effects from the top of the device are exaggerated, the need for an air gap becomes more relevant. Also, the dip that began at h = 25 W/m^2-K is more significant at higher convection coefficient values.

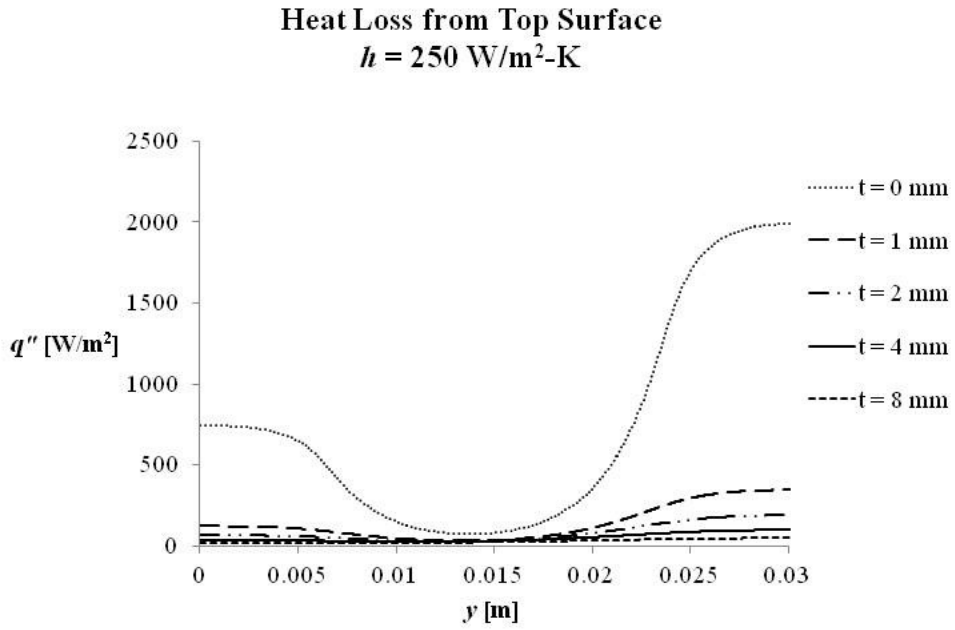

Figure 4.13: The heat lost from the system with the maximum convection effects and without an air gap are now 66.6 times larger than what was observed with the minimum convection coefficient of 2 W/m^2-K. The heat loss from the systems with an air gap has also increased, but not as drastically.

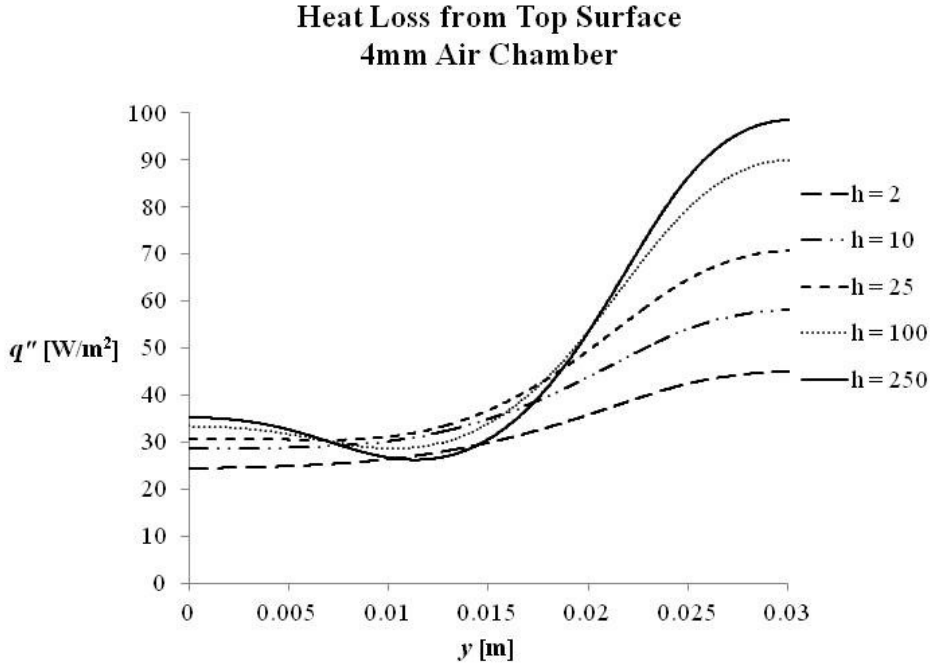

Figure 4.14: With the air gap thickness being held constant at 4mm, the effects of convection on heat loss can be directly analyzed. As expected, with a larger amount of convection, there is more heat loss from the system.

The profiles shown in Figure 4.11 begin to show a dip in the center of the device showing there is less heat being lost from the center of the device than above the heaters. The dip is noticed when the convection effects are large enough to cool the device temperature below both heater temperatures. Also, since the boundaries adjacent to the glass surface are adiabatic, the heat flux gradient, dq''/dy, is zero at both ends of the glass slide. This is a realistic assumption since the glass slides will sit in a polycarbonate cover during experimentation. In general, the heat loss increases with increasing y due to the increasing temperature observed along the temperature gradient.

An interesting phenomenon is observed in Figure 4.14, where the heat loss increases as h increases, as expected, over the two heaters. The lower thermal resistance associated with the high h increases the conduction directly to the top surface, resulting in less heat transferred to the region between the heaters. This phenomenon is evidenced by the dip in the heat flux from the top surface for the mid-range x values.

From these plots it is clear that as the convection effects increase, more heat is lost and as the air gap thickness increases, the heat loss decreases. Therefore, the ideal system would be able to achieve a temperature gradient as close to linear as possible, which is observed in systems with a large air gap thickness and low convection conditions.

Conduction is by far the most prevalent mode of heat transfer seen in this system; however, convection and radiation play a large role in determining how much heat is lost, which turns out to be crucial to the success of the device. The presented simulations suggest that radiation dominates the amount of heat lost until a certain point when

convection reaches a large enough value to override radiation. Therefore, it is essential that both are included in the simulations.

4.3 Periodic Flow Condition

With the simulation validated and a 2D model solved, a more robust simulation is created to observe how the convection and radiation affect the fluid dynamics in the system. An infinite number of cycles are assumed in this simulation, which will provide information about the temperature difference between the fluid and device surface, without making the assumptions made in Chapter 3. Most importantly, however, is that this simulation is capable of aiding in optimizing heater set-point temperatures for a specific flow rate.

One PCR cycle is modeled with the air gap and glass on top. Periodic heat boundary conditions are applied to the right and left sides of the system. The heater temperatures are defined at the heater interface with the device above and below the fluid channel and are optimized for each flow rate. An inlet velocity is defined so the fluid experiences flow rates between 0.1 and 1 mL/hr. Convection and radiation act on the top surface while conduction and radiation act between the device and glass surface. Convection on the top surface is defined as the lowest natural convection experienced, with h = 2 W/m^2-K. Results from the 2D simulation are used to show the trends as the convection effects are increased. In this model, all regions which do not have an isothermal, convection, radiation or periodic boundary condition are considered to be adiabatic. These boundary conditions are summarized in Figure 4.15.

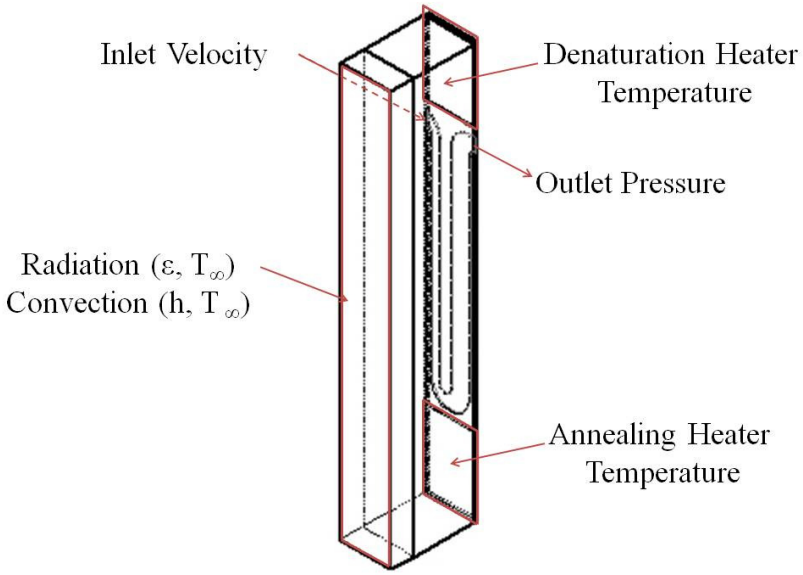

Figure 4.15: Boundary conditions for the out-of-flow-plane heat transfer analysis with periodic boundary conditions to represent a system with an infinite number of PCR cycles.

4.3.1 Mesh Refinement and Convergence Criteria

Unlike the two-dimensional simulation, this model includes fluid motion, requiring the mesh to be based on the velocity. A model with 935350 mesh elements was used to analyze the out-of-flow-plane heat transfer. A simulation with 1114638 mesh elements was also solved to verify mesh independence. If the maximum velocity from the two mesh cases results in less than 2% error, the solution is assumed to be fully converged. The actual error found was 1.9%. Although this is on the high end of assumed convergence, this model will be validated with experimental data in Chapter 5. The same convergence criterion as defined in the 2D model is used for this study.

4.3.2 Periodic Results

4.3.2.1 Optimized Heater Temperature and Flow Rate

The defined simulation is solved with h = 2 W/m^2-K and included radiation off the top surface. The inlet velocity is varied and a range of heater temperatures are found which allow the fluid sample to reach the desired temperature ranges in the reaction locations throughout the device. These heater temperature set-points for a given flow rate are defined in Figure 4.16 for the denaturation side and Figure 4.17 for the annealing side.

Figure 4.16 suggests that as the flow rate increases, the denaturation heater must also increase its temperature to achieve the desired reaction temperatures. Intuitively, this makes sense since as the velocity increases, less time is given for the fluid to reach the desired temperature before moving onto the next reaction; therefore, there must be more heat present. Figure 4.17 shows that there is little correlation between the annealing temperature settings and the achieved sample temperature. An important result from this model, which is not represented in these figures, is the decrease in temperature in the center of the device, similar to that observed in the 2D model. With the device losing heat, it is able to achieve the annealing temperature without a large dependence on flow rate.

4.3.2.2 Fluid to Surface Temperature Correlation

Since the system temperature is measured with an IR camera, only the top surface temperature of the device will be recorded. Therefore, two methods are presented to find

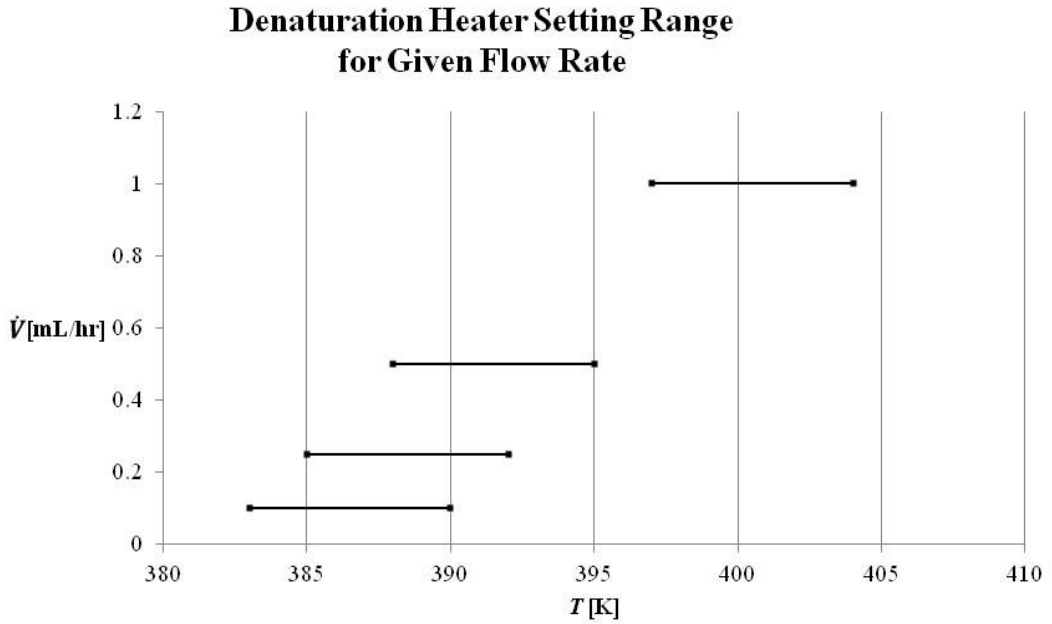

Figure 4.16: Acceptable heater temperature range for denaturation side to allow the fluid temperature to reach a value between 90°C and 96°C.

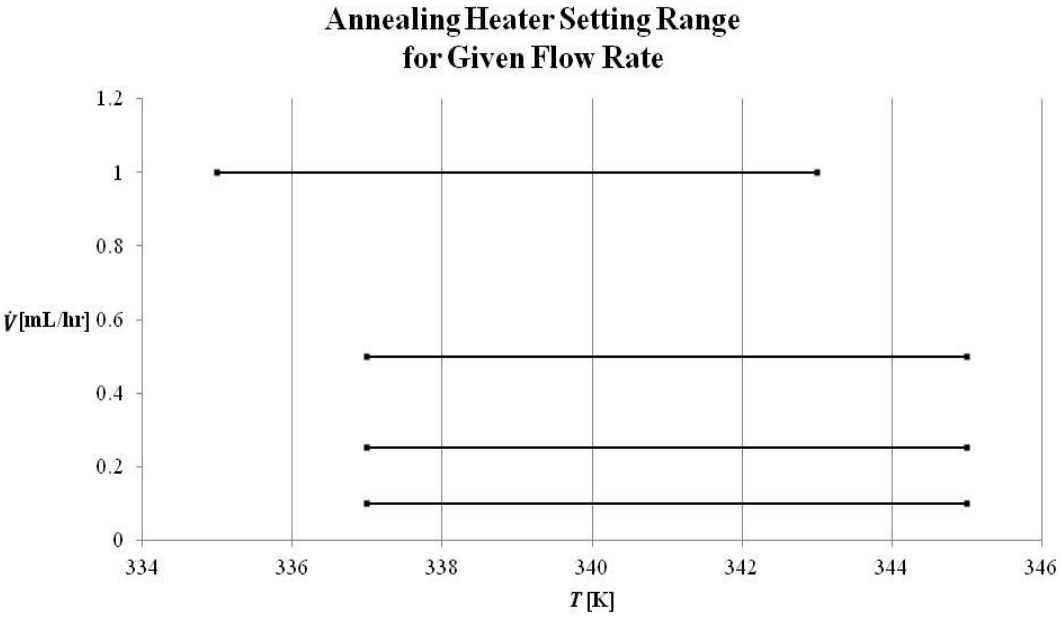

Figure 4.17: Acceptable heater temperature range for the annealing side to allow the fluid temperature to reach a value between 58°C and 65°C.

the difference between the fluid and surface temperature. The first method for determining the relation between fluid temperature and device temperature comes from Eq 4.12 which is based on an energy balance between the convection removing heat from the surface of the device and the conduction occurring between the fluid and device surface.

$$T_f = \left(\frac{Lh}{k} + 1\right)(T_s - T_\infty) + T_\infty \qquad [4.12]$$

where T_f is the temperature of the fluid, L is the distance from the device surface to the center of the fluid channel, h is the convective heat transfer coefficient at the device to air interface, k is the thermal conductivity of the PC material, T_s is the surface temperature and T_∞ is the ambient temperature.

The lowest natural convection coefficient, h = 2 W/m^2-K, is used for this calculation to match experimental conditions. In practice, the glass slide is carefully slipped off, exposing the top of the device to the thermal imaging camera, resulting in very little induced convection. Since the surface temperature will vary through the device due to the established temperature gradient, this calculation is completed for a range of surface temperatures. The difference between the fluid and surface temperatures for a typical range of surface temperatures is shown in Fig. 4.18.

From Figure 4.18, it is observed that although the difference in fluid to device temperature increases with an increase in device temperature, the maximum difference is approximately 0.14°C.

Eq. 4.12 does not take into account the fluid motion. To examine if flow rate has

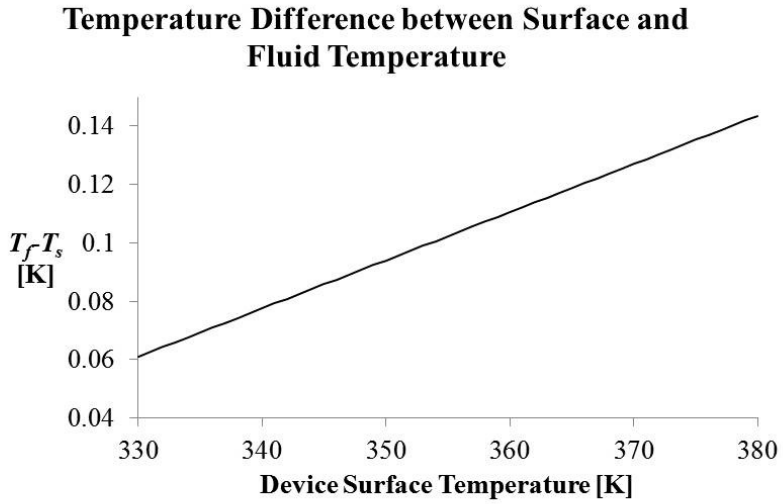

Figure 4.18: The fluid and surface temperature difference as a function of the device surface temperature.

an impact on fluid-to-surface-temperature difference, nodes are created both inside the channel and on the surface at the same *x* and *y* locations. The denaturation points are examined first. For flow rates below 0.5 mL/hr, the average temperature difference between the fluid and surface is less than 0.07°C. When the flow rate is increased, there is not enough time for the fluid to change temperature, resulting in the surface temperature being greater than the fluid temperature on the denaturation side. For 1mL/hr, the fluid in the denaturation bend is 0.3°C less than the surface temperature. This trend was not noticed on the cold side, most likely due to the decrease in heat loss throughout the center. Even with the largest temperature difference being approximately 0.3°C, the resolution of the IR camera is less than this, so the difference observed between the center of the fluid channel and the device surface can be neglected.

4.3.2.3 2D, 3D Simulation Comparison

The heat loss predicted by the 2D model without any fluid motion is compared to the periodic 3D system data in Figure 4.19 using the glass surface temperatures. It appears the 3D system with periodic flow loses less heat to the environment, most likely because energy from the system is also allowed to leave with the fluid as opposed to just out the top surface. However, the trends are the same for the two simulations, making the results for the 2D simulation directly applicable to the 3D system.

4.4 Discussion

By simulating the heat transfer occurring in the device, considerable insight of system behavior can be developed. First, the heater temperatures discovered in Chapter 3 do not take into account how much heat the system is losing, but the

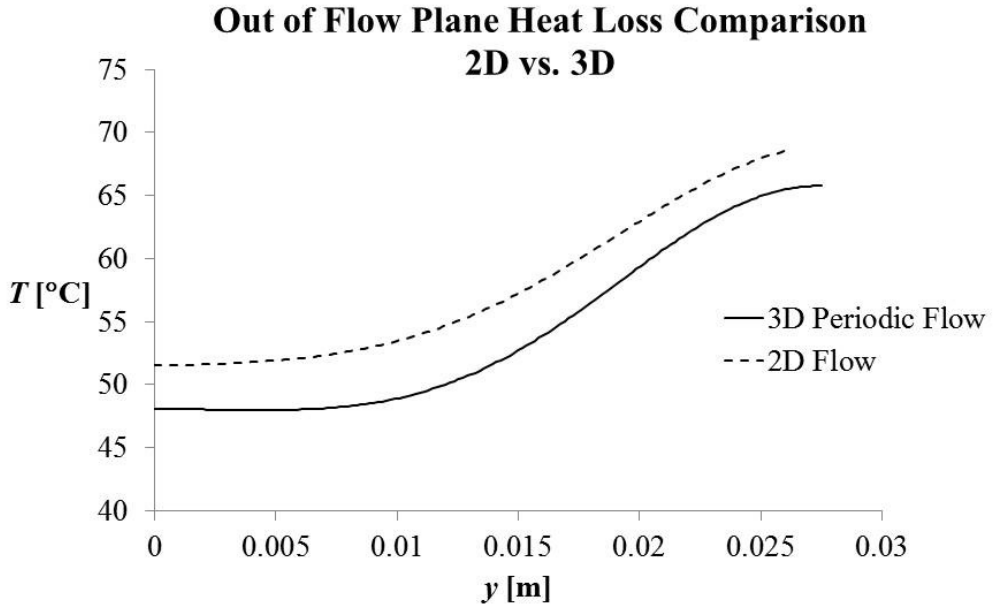

Figure 4.19: Glass surface temperature comparison of two simulations completed; the 2D without fluid motion and 3D with a periodic flow condition.

simulations presented here show that heater set-point temperatures do depend on the sample flow rate and can be predicted fairly easily. Second, the sample temperature is on average only 0.10 ºC warmer than the device surface temperature. This also shows that the assumption made in Chapter 3 to neglect the upper and lower layer of PC to simplify the problem is valid. Third, the heat lost from the system can be reduced by increasing the air gap thickness, or reducing convection from the top surface of the system. Lastly, the simulations presented in this chapter confirm that PCR reaction temperatures can be achieved in a polycarbonate device.

CHAPTER 5

EXPERIMENTAL METHODS AND RESULTS

Experimental data are needed to validate that the results produced by the simulations are correct. A fixture was created to closely match the simulation conditions. Water was run through the device to more closely represent the simulation and several PCR samples were also run through the device to verify that PCR was occurring. IR images were taken of each test and an end point PCR analysis was performed on all the PCR samples. The thermal images produced results suggesting the PCR reaction temperatures were being reached; however, due to significant flow rate inconsistencies, PCR was unsuccessful. In order to fully understand what was occurring during the experiments, the periodic flow simulation was revisited and the convection and flow rate parameters were changed until the temperatures produced matched the experimental conditions. This simulation could be used in the future to predict the device behavior.

To accurately replicate the simulated conditions, a fixture was created to hold and heat the microfluidic device while providing insulation below and around the top of the device, and allowing the center of the device to be exposed for IR temperature measurements. To perform the experiments, a temperature controller, power supply,

syringe pump, IR camera, heaters and temperature sensors are required in addition to the fixture and device.

5.1 Fixture

The experimental fixture, shown in Figure 5.1, consists of a Teflon piece providing insulation to the bottom of the device, a polycarbonate cover creating insulation around the top of the device, and removable glass slides coated in black spray paint (not shown) closing the gap above the device. The glass slides are spray painted black to increase the emissivity of the glass, thereby increasing the accuracy of the IR images of the glass surface. Without the paint, the image is taken somewhere in between the device and glass. In Chapter 4, it was found that as the air gap thickness was doubled, the heat lost would decrease linearly showing diminishing returns. A 4mm air gap thickness was chosen for use in the experimental setup because it proved to be the most efficient while reducing the amount of material used.

5.1.1 Heaters/ Temperature Control

One of the most important design considerations for this device is being able to establish the thermal gradient. To apply a temperature gradient across the device, two $10W/in^2$, 1" x 6" resistive heaters (Omega SRMU 100106) are in contact with the bottom of the device, one above and one below the fluid channel. The heaters are positioned so the resistive heating element is just 0.5mm from the fluid channel for reasons discovered in Chapter 3. Both heaters are powered independently by a DC power supply (Tektronix PS280) and maintained at the designated temperatures with a temperature

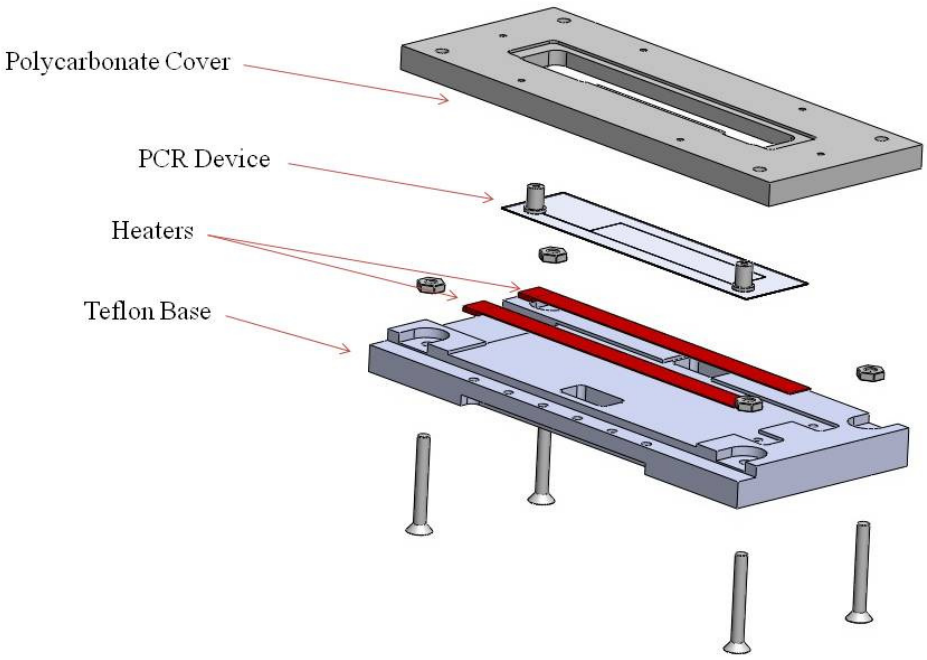

Figure 5.1: Exploded view of experimental fixture. The primary purpose of this system is to insulate the device and heaters as efficiently as possible. The entire system is secured with winged bolts to ensure good thermal contact.

controller (Omega CN 4216-R1-R2) which provides a feedback loop between the power supply and temperature sensors. The temperature sensors (Omega IRCU-010) are placed on top of the PC device, as close to the channels as possible and secured with Kapton tape.

5.2 Thermal Imaging

A temperature measuring system must be incorporated into the experimental system to ensure the PCR sample is achieving the expected reaction temperatures. Incorporating temperature sensors into the fluid channel is not feasible with the manufacturing process and any protrusion into the channel would disrupt the flow. Thus, a noninvasive IR camera (Inframetrics PM 390 Thermacam) is used, but the IR camera is only able to record the surface temperature. The IR camera must be directed towards the

device surface at a slight angle to eliminate the possibility of the cooling apparatus inside the camera being reflected into the images. The camera needs line of sight vision to the device, requiring the glass slides used as insulation to be removed just before an IR image is taken. The slides are carefully slipped off laterally to prevent additional convection effects from forming and the image is taken as quickly as possible. In general, the slides are removed for no more than 4 seconds before the image is taken. A lumped capacitance calculation, shown in Eq 5.1, is used to analyze how much the surface temperature decreases during the few seconds that the glass slides are removed.

$$\frac{\mathrm{T}-\mathrm{T}_{\infty}}{\mathrm{T}_{\mathrm{i}}-\mathrm{T}_{\infty}}=\exp\left(-\left(\frac{hA_s}{\rho\forall c}\right)\tau\right) \qquad [5.1]$$

If the initial surface temperature of the device is 375K, which is approximately the average across the device, and h is assumed to be the lowest possible natural convection coefficient, 2 W/m^2-K, the surface temperature of the device after the glass is removed is shown in Figure 5.2 for the first 10 seconds. An expected exponential trend is found as time is increased, but the trend appears linear during the first several seconds. The convection coefficient can be assumed to be so low since the glass is slowly removed laterally, creating minimal convection effects in the chamber above the device.

It is clear from Figure 5.2 that removing the glass slides, even for up to 10 seconds, has only a small impact on the device surface temperature since the device temperature is expected to drop less than one degree during those first 10 seconds. The glass is generally removed for less than 5 seconds, so this heat loss can be neglected as long as the surface temperature measured is not within 0.5 °C of the reaction temperature

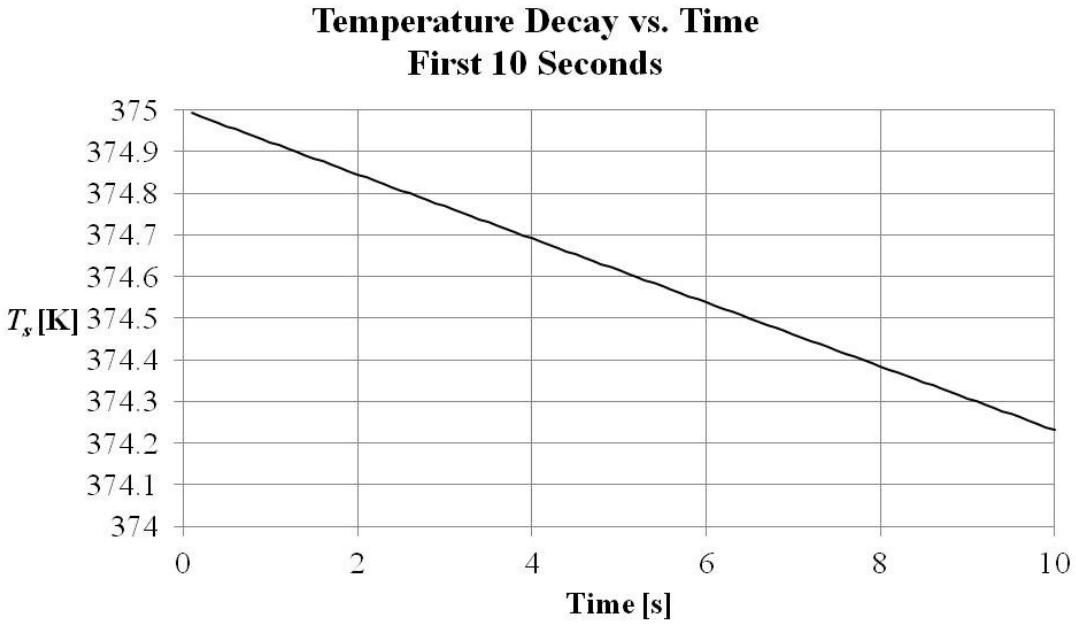

Figure 5.2: The temperature decrease as glass slides are removed from the system. It is seen that after only 10 seconds, the temperature drops approximately 0.8K.

limits. This calculation does not consider the water in the channel. From experience and previous simulations, it is unlikely the water in the channel is affected by the removal of the glass slide. There simply is not enough time for the surface temperature variation to penetrate into the fluid.

To obtain an accurate measurement from the IR camera, the camera must be in focus, and the emissivity of the material must be known. The emissivity of a material can be determined with the IR camera by allowing a piece of electrical tape, which has a known emissivity of 0.98 [35], and the material with unknown emissivity to reach the same steady state temperature. The spot feature is used on the IR camera, which displays the temperature at a specific point that can be moved throughout the image. With this feature enabled and the emissivity set to 0.98, the temperature of the electrical tape is recorded. Then, the point is moved to the material of interest and the emissivity is adjusted until the temperature displayed matches the temperature of the electrical tape.

The painted glass slides were found to have an emissivity very close to 1 and the PCR device has an emissivity of about 0.99.

5.3 Experimental Procedure

With the device manufactured from procedures outlined in Chapter 2 and the experimental setup prepared, the device is placed in the fixture, ensuring correct placement of the heaters and temperature sensors. The device is positioned on top of the heaters with the heating element as close to 0.5 mm from the channel as possible for reasons discussed in Chapter 2. Then, the temperature sensors are placed on top of the heating elements. The PC cover is put into place and the fluid ports are attached. With the system tightly secured with bolts and the glass slides placed above the PC cover, the power supply is turned on. The denaturation heater is set to 115°C and the annealing heater temperature is set to 56°C. These temperatures vary slightly from the ranges found in Chapter 4 and reasons will be discussed with the results. The device is allowed to reach steady state before the water is pumped through the device. To ensure a steady state thermal gradient is achieved, IR images are taken periodically throughout the heating process and the change in maximum temperature is recorded. When this temperature changes less than 0.1K over an hour, the device is considered steady state. Then, water is pushed through the device at 1 mL/hr.

5.4 Postprocessing – IR Images

IR images are stored on a removable memory stick then imported into post-processing software, TherMonitor, created specifically for the IR camera. This software

is capable of plotting the temperature data along a user-defined line, which can then be used as a means of comparison to the simulation results. Images of the device surface are taken, allowing easy comparison to the results from the simulations.

5.4.1 Thermal Results

An actual IR image of the device with fluid being passed through the channel is shown in Figure 5.3 where the black outline represents the device in the image, the denaturation heater is at the top and the annealing heater is at the bottom. The observed color ‘spikes’ arise from the fluid carrying the heat from the denaturation heater side to the annealing heater side. Two lines are drawn signifying where the program will analyze the temperatures. For each pixel along the drawn line, a temperature can be determined. After extracting this temperature data, values were chosen representing the point on the device surface above the locations where they were observed from the COMSOL model. The denaturation and annealing temperatures are displayed in Figures 5.4 and 5.5, respectively. Each of these curves shows an increase in temperature at the center of the device. Three explanations for this feature are end effects, heater inconsistency and/or the location of the glass slides. Since end effects were not analyzed in a full 3D model, it is unknown if this increase and decrease in temperature is expected or not. The 6” long heater may not be producing a constant temperature throughout its length, potentially resulting in covered by a glass slide; however, during the experiments, tubes were required to deliver and collect the fluid, requiring an open areas around the nanoports and allowing space for a glass slide to only cover the area directly above the channels. Any one of these, or a combination of the three possible error sources, could have resulted in

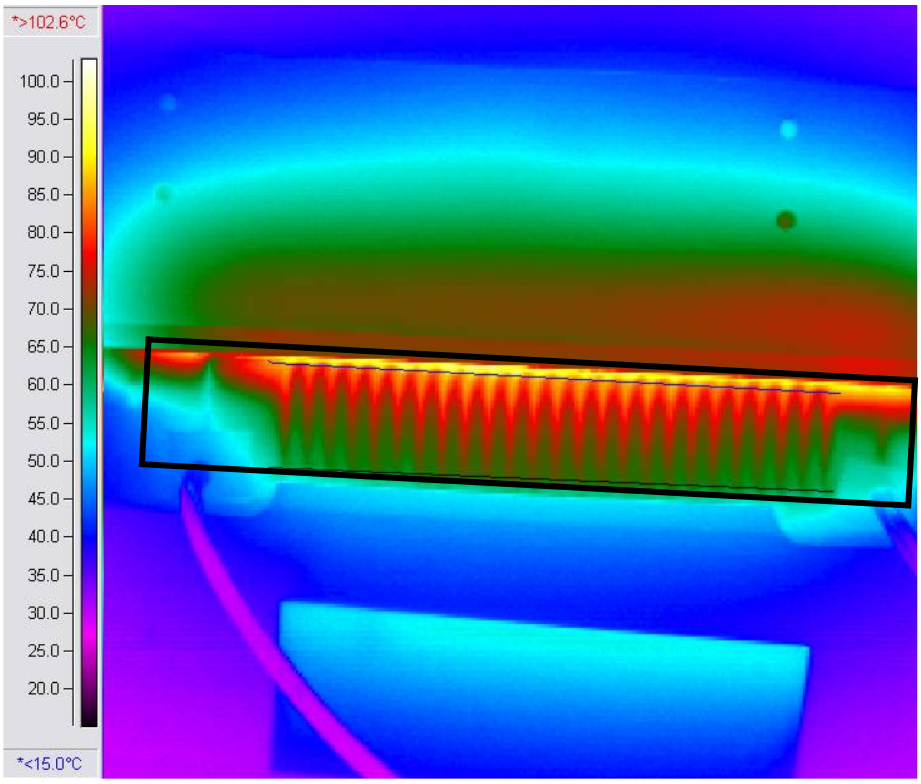

Figure 5.3: IR image of device surface with water flowing through the channel. The device is outlined in black. Heat is being carried from the denaturation heater side (bottom) to the annealing heater side (top) and is realized as 'spikes.

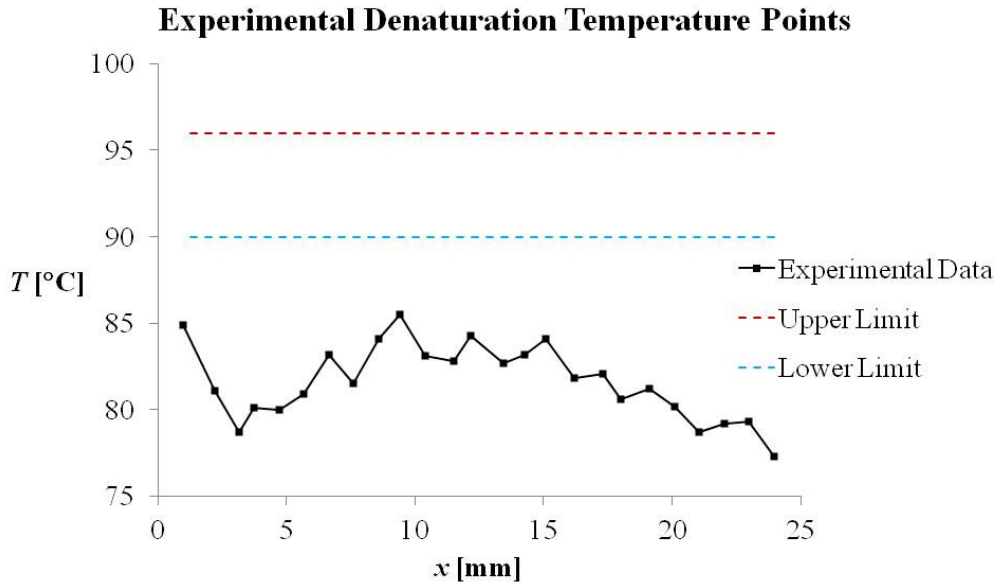

Figure 5.4: Experimental denaturation temperature data for the points on the surface of the device directly above the bends in the channel where the temperature was analyzed in the COMSOL models

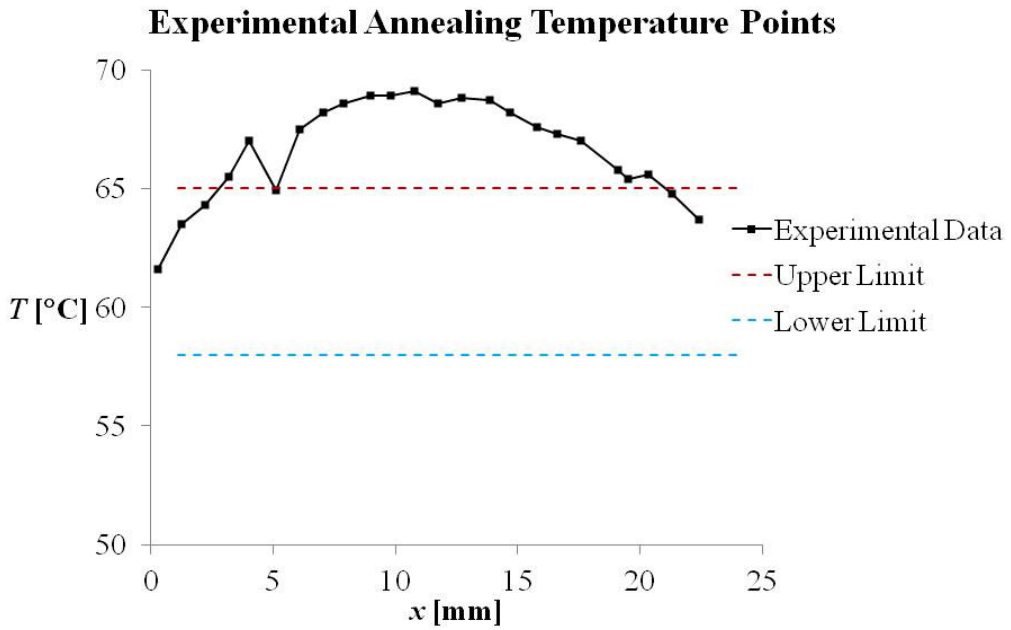

Figure 5.5: Experimental annealing temperature data for the points on the surface of the device directly above the bends in the channel where the temperature was analyzed in the COMSOL models

the observed temperature 'hump.'

It can be seen from Figures 5.4 and 5.5, and by recalling the assumption that the temperature along the surface is nearly identical to the actual fluid temperature, that the fluid temperature along the length of the device rarely reaches the PCR reaction temperature limits.

As previously mentioned, the heater temperatures were not within the range specified in Chapter 4. This range was not reached because at temperatures higher than 115°C, evaporation was observed in the channels. In an attempt to compensate, the annealing heater temperature value was increased. To validate the 3D periodic simulation created in Chapter 4, the experimental conditions are applied to the model and results can be compared. The simulation will produce one temperature for denaturation and one for annealing, representing the channels in the center of the device.

The simulation produces a denaturation temperature of 91.7°C and an annealing temperature of 60.4°C with the experimental conditions of 1 mL/hr flow rate, denaturation heater temperature of 115°C and annealing heater temperature of 56°C. If the experimental values in the center of the device are averaged, denaturation and annealing temperatures of 83.1°C and 68.6°C are found, respectively. These results show a significant discrepancy between the experiment and simulation, implying either the flow rate in the experiment is actually faster than prescribed or the simulation did not accurately represent the experimental conditions. In the first case, flow rate faster than expected can be assumed because the temperature difference between the denaturation and annealing temperatures is smaller in the experiment, signifying the fluid had less time to change temperature and was therefore traveling faster than expected. If the flow rate in the simulation is increased to 2.1 mL/hr, denaturation and annealing temperatures are found to be 83.4°C and 67.4°C, respectively. This produces an error of less than 2% and validates the simulation to be true. These results are summarized in Table 5.1.

One reason for the experiment not reaching the reaction temperatures is the flow rate could have been faster than desired when the IR image was taken. It should be noted

Table 5.1 Summary of experimental and simulation results. For each of these, the denaturation heater temperature is assumed to be 115°C and the annealing heater temperature is assumed to be 56°C.

Parameter	**Experiment**	**Simulation**	
Volumetric Flow Rate [mL/hr]	"1"	1	2.1
Denaturation Temperature [°C]	83.1	91.7	83.4
Annealing Temperature [°C]	68.6	60.4	67.4

that according to the simulation, if the correct flow rate had been applied in the experiment and the thermal gradient was consistent, then the PCR reaction temperatures would have been met. This proves that there are many more heater temperature combinations available to reach the reaction temperatures than defined in Chapter 4. Further experimentation must be completed in order to conclusively state that inconsistent flow rates are the only explanation for the discrepancy between experimental and simulation results.

5.5 PCR Experimental Procedure

With the IR images closely matching the data produced from the simulation, several PCR tests are completed to determine if DNA is being amplified. A procedure similar to the water experiment is followed for the PCR test. One addition to this process is the passivation of the PC channel. Since PC is predominantly hydrophilic, a surface passivation step is required prior to addition of heat and the PCR reactants, for reasons discussed in Chapter 1, before the device is capable of performing PCR. To accomplish this, 0.3 mL of a 1% PVP to nuclease-free water mixture is pumped through the device at a flow rate of 0.3 mL/hr. The channel is then rinsed with 2.5 mL of nuclease-free water at a flow rate of 2.5 mL/hr with a 2.5 mL glass syringe (Hamilton Gastight #1002) to ensure all the PVP has been removed.

The heaters and temperature sensors are arranged as previously discussed. Table 5.2 summarizes the various flow rates and heater settings used. The power source is turned on and the device is allowed an hour and a half to reach steady state. While the device is reaching steady state, the PCR sample is prepared. The PCR sample used for

Table 5.2: Summary of temperature set-points used for the different flow rates during experimentation.

Flow Rate [mL/hr]	**Heater Temperatures**	
	Denaturation [K]	**Annealing [K]**
0.1	388	327
0.25	385	327
0.5	384	329
1	384	329

testing includes a DNA segment of interest with 70 base pairs. One part DNA (5x Mix 2mM, +Ab) is mixed with one part Primer 1 (CVBB x10 SAF), one part Primer 2 (CVBB x10 SA R), two parts nucleotides (RP DNA) and five parts nuclease-free water.

The sample is kept refrigerated until the device reaches steady state. To ensure the sample is completely mixed just before testing, the sample is placed on a vortexer (VWR MV-1 Mini Vortexer) for 2 minutes. Just before the sample is added to the channel, 10μL of glycerol is partially pulled through the system to prevent the formation of bubbles and make the flow rate more consistent [36]. As the glycerol is moving through the channel, 20μL of the PCR sample is added and pulled through the device at a constant flow rate with a 100mL glass syringe (Hamilton Gastight #1010). Due to the small sample size, the sample does not fill the entire channel. Since the 3D periodic flow simulation assumes there are no end effects, an IR image is taken when the sample is near the center of the device to collect data for simulation comparisons. Once the sample has traveled through the entire channel, the volume is collected in a small vial then analyzed for PCR efficiency afterwards.

Although the device is designed to be disposable, it can be reused if an appropriate cleaning protocol is completed between each PCR test. After the PCR sample

is passed through the channel, 1 mL of 1% bleach to nuclease-free water is pushed through the channel at 1 mL/hr. The channel is then rinsed with 2.5 mL of nuclease-free water for 1 hour. Now the procedure can be followed as if the device was new.

5.5.1 Thermal Results

Although the sample was expected to be pulled through the channel at a consistent flow rate, the observed flow rate varied greatly. From experimental observation, the sample plug would be stationary for a prolonged amount of time (30-60 seconds), then suddenly travel very quickly, higher than the intended flow rate. The reasons for such anomalies are attributed to the pressure difference between one end of the channel (atmospheric) and the other end (in the syringe). The maximum pressure difference possible is atmospheric pressure; however, a greater pressure is required for the sample to experience a consistent flow rate. This could be achieved by pushing the fluid through the channel, as opposed to pulling, producing a greater pressure different between the inlet and outlet or using a smaller syringe to increase the accuracy of the syringe pump.

In addition to the obvious impacts on DNA amplification that the flow stopping and starting again will cause, another significant consequence is evaporation. The heater temperatures are defined assuming the fluid is constantly moving. If the sample is stalled for any amount of time, heat is able to travel into the fluid and cause boiling, leading to evaporation, which causes vapor bubbles. These unintended vapor pockets add to the pressure problems and hinder the flow progression. As mentioned, the heater set-points defined in Table 5.2 for a flow rate of 1 mL/hr are not within the range defined in

Chapter 4 for successful PCR reaction temperatures to be met within the channel. The reason for this discrepancy is that when the experimental temperatures were increased past these temperatures, the abnormal flow rate behavior was amplified. Also, in an attempt to reduce the amount of evaporation when the sample was not moving, the heater temperatures were reduced.

To compare the fluid temperature within the channel of the simulation to that of the experiment, a line is carefully drawn which closely intersects the channel turns at both the top and bottom, similar to the data collected from the simulations. However, drawing a line in the IR image also collects temperature data from the PC material between the channels, which is not included in the simulation results. It is important to be able to differentiate if the temperature in the plot is above a fluid channel or from the PC material between them. Unlike the water experiments, the channel points were not extracted from the entire set of data. On the denaturation side of the chip, it is known that the lower temperatures are generated by the fluid while the peaks are from the device since the device is hotter than the fluid. Conversely, the peaks measured on the annealing side correspond to the fluid channel where the minimums correspond to the device since the fluid is carrying more heat from the denaturation side than the annealing side would normally experience.

Although the flow rate was not always consistent, the flow rate did perform as expected sporadically. The cycle time for each test was measured and when the correct flow rate occurred, the IR image was taken. The results from the IR images are shown in Figures 5.6 and 5.7 for the denaturation and annealing side, respectively. Recall that the

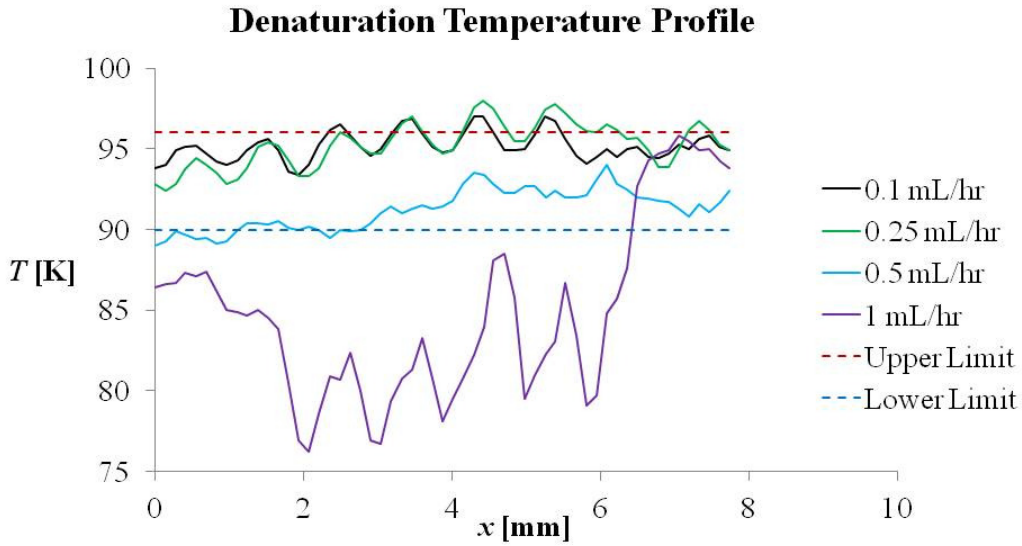

Figure 5.6: Temperature data across the denaturation bends of the device from experiments with four flow rates. This information takes into account the PC temperature as well as the channel temperature, so the troughs represent the device temperature just above the fluid channel.

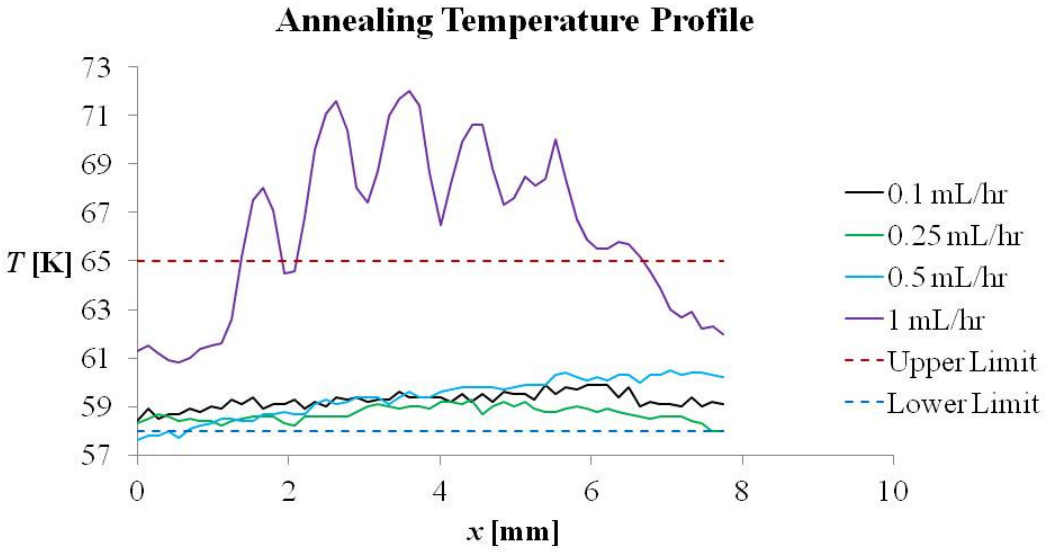

Figure 5.7: Temperature data across the annealing bends of the device from experiments with four flow rates. This information takes into account the PC temperature as well as the channel temperature, so the peaks represent the device temperature just above the fluid channel.

bottoms of the denaturation plot and the peaks of the annealing plot are the fluid temperatures.

These results show that with a flow rate equal to or less than 0.5 mL/hr, the temperatures are within the PCR reaction temperature limits, or could easily be adjusted to fit within the limits. The temperatures used for the 0.5 mL/hr flow rate were on the lower limit of the allowable heater temperature range found in Chapter 4, so they are expected to be just within the temperature limits. In the denaturation plot, there are two points slightly below the lower temperature limit. This deviation from the simulation is likely due to either the inconsistent flow rate or slightly varying lab environmental conditions than those defined in the simulation.

With a flow rate of 1 mL/hr, neither the denaturation nor annealing reaction temperatures are met within the sample. This may be expected since the heater values required to reach the reaction temperatures for a flow rate of 1 mL/hr from Chapter 4 were approximately 9°C higher than the values used; however, the fluid temperature changes less than 8°C on average between the annealing and denaturation regions. Recall the simulations with a flow rate of 1 mL/hr were able to produce sample temperatures within the reaction limits for annealing (58°C-65°C) and denaturation (90°C-96°C). Therefore, the average temperature difference between these reaction temperatures should be at least 25°C. A difference of less than 8°C suggests that the flow rate in the image is faster than expected.

5.5.2 Simulation with Updated Experimental Conditions

To determine the exact experimental conditions, including the flow rate and convection coefficient, the periodic flow simulation used in Chapter 4 was revisited and the PC cover pieces were added to accurately match the experimental platform, as shown in Figure 5.8. Using experimental heater temperature values, the convection parameter, *h*, and flow rate were varied until a valid comparison between the simulation and experimental results were obtained for a flow rate of 1 mL/hr, since this was the most unpredictable. To provide another metric of comparison, the IR images taken of the glass slides when the experimental system was at steady state are compared to the temperature gradient result from the simulation.

The flow rate in the simulation had to be increased to 3 mL/hr with a convection coefficient of 2 W/m^2-K, in order to obtain similar results. The device temperature above the denaturation location was found to be 77.7°C from the simulation, which can be compared to the experiment by taking an average of the temperatures in this region,

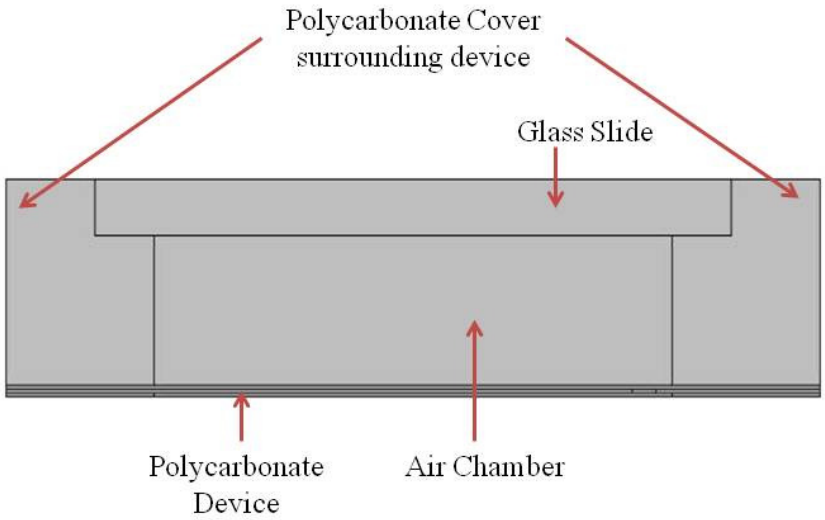

Figure 5.8: Cross-section of verification model. The same periodic boundary conditions are applied to this model as discussed in Chapter 4.

which resulted in a temperature of 77.9°C. The same procedure was taken for the annealing side with a simulation result of 69.9°C and an experimental result of 70.4°C. The fluid temperatures match within less than 0.8%. Although the flow rate was assumed to be 1 mL/hr experimentally, it was found to actually be 3 mL/hr despite attempts to take the IR image when the measured cycle time matched the calculated cycle time. This extremely fast flow rate result contributes to why the measured temperatures were not within the reaction temperature limits as expected.

With the simulation able to match the results from the experiment, this updated simulation is deemed a good characterization of the experiment. This simulation may now be trusted for further analysis, especially including any channel geometry design changes.

5.5.3 PCR Results

To test if PCR was completed in the samples which were run through the PC device, a standard melting analysis was completed. The details of this procedure are outlined in Crews' dissertation [26]. For comparison, in addition to the four samples cycled in the PC device, two positive control samples were amplified in the LightCycler, a commercial PCR testing device. One of these samples was directly from the lot of PCR mixture used in the experiments, and the other was from the same lot but passed through the PC device without any heat to ensure any PCR failure is not due to the surface effects.

The results for the defined PCR tests were all unsuccessful; however, this is likely due to the variation in experienced flow rate. Another set of PCR samples were run with the parameters specified in Table 5.3 with improved, but not perfect, flow rates and

Table 5.3: Experimental conditions used during another set of PCR tests

Sample	Flow Rate [mL/hr]	Heater Temperatures	
		Denaturation [K]	Annealing [K]
1	1	380	320
2	0.5	380	322
3	1	388	327
4	0.5	388	327

compared to a positive control sample run through the LightCycler. The melting analysis result for the positive control is shown in Figure 5.9. The results from the sample tests are shown in Figure 5.10.

From Figure 5.10, it is clear that Sample 1 and 2 did not achieve PCR. It appears that Samples 3 and 4 are closer to achieving a useable PCR; however, the process is still not successful. The melting temperature for Sample 3 is approximately 77.3°C, where the melting temperature for the positive control was approximately 79.8°C. With the discrepancy of temperature associated with the peak of the results and the vastly different shapes to the curves, PCR was not achieved as desired.

5.6 Discussion

Due to significant flow rate inconsistency problems experienced during testing, the tests conducted were largely unsuccessful. However, improving the flow rate consistency by using a smaller syringe and pushing the fluid through the channel opposed to pulling, it is anticipated that this PC device is capable of reaching the PCR reaction temperatures on the presented simulations and promising thermal images.

Recall the channel geometry presented in this thesis is based on the work of Niel Crews' glass CF-PCR device. It appears each material has its advantages. Glass is able to

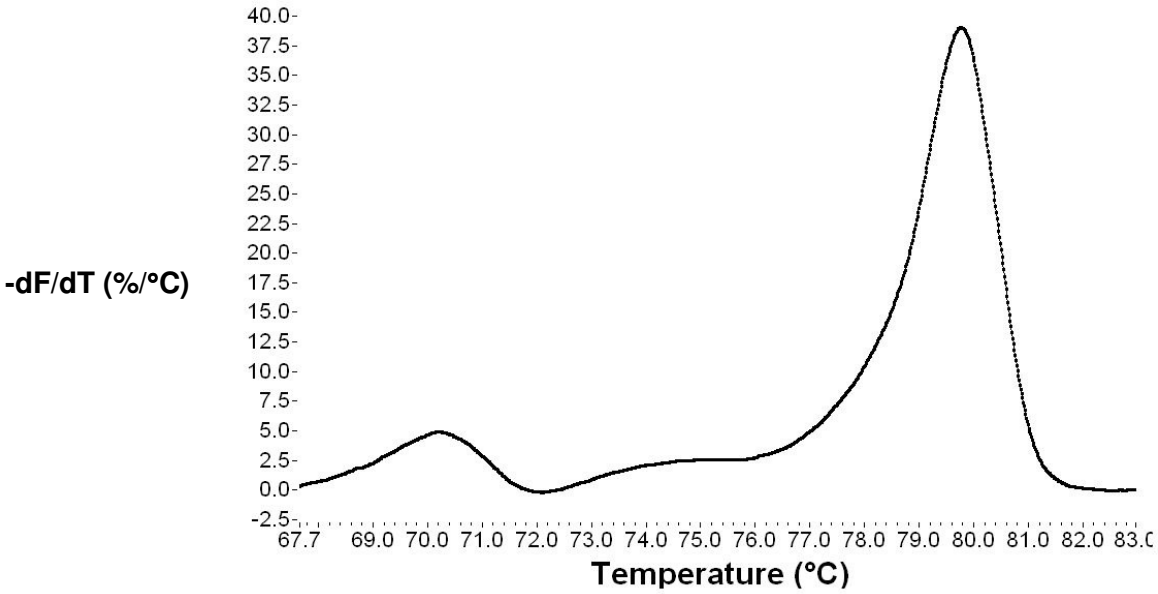

Figure 5.9: Melting analysis result for positive control

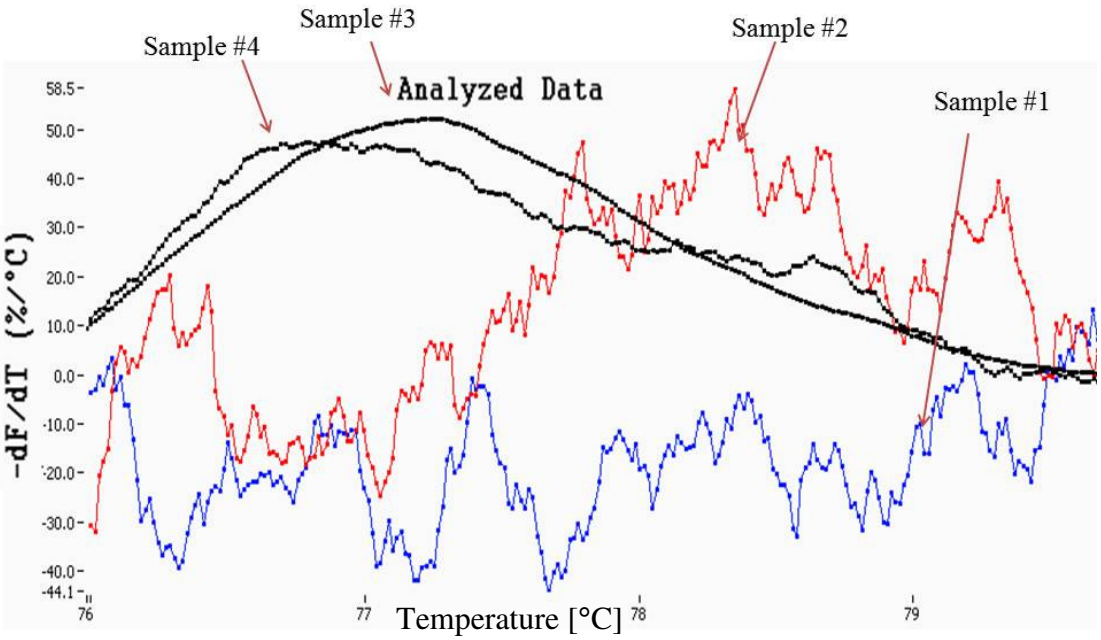

Figure 5.10: Melting analysis result for all four samples

achieve a steady state temperature gradient quicker and has a smaller area footprint. Polycarbonate is cheaper to purchase and manufacture, does not require a microfabrication facility and is able to achieve a more uniform temperature gradient. Both are able to achieve PCR reaction temperatures in comparable cycle times.

CHAPTER 6

CONCLUSIONS

A disposable, polycarbonate CF-PCR device was developed and analyzed in this work. From simulations and experimental IR data, it was shown that DNA amplification could be achieved at slow flow rates and it is optimistic that with slight adjustments to the test platform, higher flow rates could also prove successful. The heat transfer being lost from the system was also analyzed and shown to have a significant impact on the overall system performance.

6.1 Results

Through the process of developing this device and the simulations to predict its behavior, many scientific findings and engineering applications were discovered. These include:

- **2D simulations are not a good approximation for this 3D microfluidic system:** Simulations of the flow plane were created in 2D and 3D. The temperature was measured in the denaturation and annealing reaction regions at each bend. When the temperatures were compared, the trends were the same, but the values were significantly different.

- **Heater proximity to the fluid channel has a significant impact on the established thermal gradient:** Using the concept that the trends are important in 2D and largely neglecting the actual temperature values, two 2D simulations were completed to analyze the effect of heater location. The first positioned the heaters 3 mm from the edges of the fluid channel. The second had the heaters a mere 0.5 mm away from the channel. It was found that a much more linear temperature gradient is established in systems where the heater is closer to the fluid channel.
- **Device entrance length should be designed for the specific operating conditions:** The denaturation and annealing temperature profiles of three 2D simulations were solved and compared. In this study, a very slow flow rate of 0.1 mL/hr was used and consistent heater temperatures were defined. All three entrance lengths resulted in temperature profiles within the reaction limits, and displayed a nearly constant temperature along the device. However, temperature variations were noticed during the first few reactions that would be exaggerated with increased flow rate and potentially result in these variations residing outside the temperature limits. It was found that if the entrance length is too short, the first several denaturation reactions are much lower than the constant value it became further down the channel. Conversely, if the entrance length is too long, the sample is overheated and spends the first several bends cooling off. It is ideal for the sample temperature to reach the average denaturation temperature just as it begins to travel around the first bend. This will vary based on heater temperature set-points and flow rate.

- **A completely insulated device will not reach reaction temperatures at flow rates of 1 mL/hr or higher:** A 3D simulation was completed of the center layer of the device. The entire model was considered to be insulated with the exception of the defined heater and inlet fluid temperatures. Despite numerous attempts adjusting heater temperatures in the system with a flow rate of 1 mL/hr, the fluid temperatures never reached the reaction temperatures. It was clear that there was too much heat being stored in the system.
- **PC device requires some insulation when used in windy conditions:** In extreme environmental conditions, the device will lose too much heat to operate with any accuracy and predictability. Although the lab does not experience large convection effects, an insulation system was integrated into the testing platform to analyze its behavior.
- **Including a vacuum gap above the device produces the most efficient mode of insulation:** As intuition would suggest, including a vacuum chamber above the device would cause the greatest amount of insulation. This was compared to glass directly on top of the device, an air gap, and an Argon gap. Although the vacuum gap is the most efficient, maintaining a vacuum would be difficult. Sealing around the interface and pumping the existing air out of the chamber would need to be integrated into a system for a disposable device. This would quickly become very expensive.
- **An air gap above the device is cost efficient while still providing adequate insulation:** Although the Argon chamber is the next most efficient after a vacuum chamber, the same issues of creating an air-tight integrated system would arise.

The third most efficient is the air gap. This design is easily integrated into the experimental platform and is still very efficient in insulating the device.

- **As the air gap thickness increases, the heat loss decreases:** Based on 2D simulations completed for the system with a varying air gap thickness, the amount of heat loss decreases as the distance between the device and upper glass surface increases.
- **PCR will likely occur in a polycarbonate device:** Through evaluation of the IR images taken of the device during the experiments, it is expected that DNA will be amplified in systems where the flow rate is less than 1 mL/hr. For flow rates higher than this, changes to the experimental platform or test parameters must be made.

6.2 Contributions

Through the research performed to develop this disposable, polycarbonate CF-PCR device, several contributions to the engineering world were developed.

- **2D flow plane simulation:** Several 2D simulations were developed to analyze the trends observed in the channel. Although the values for these simulations do not accurately represent the 3D model, these simulations take much less time and resources to solve and still produce important qualitative results.
- **3D flow plane simulation:** This simulation solves the fluid dynamics in the channel simultaneously with the heat transfer through the device. The model consists of the center layer and is considered to be completely insulated.

- **1D program developed in Engineering Equation Solver (EES) to analyze the heat loss through the system for four insulating scenarios:** This simple program includes all the heat transfer experienced out of the device flow plane. All the programs begin with conduction through the device, then if a gap is present, include convection and radiation for the air and Argon gaps and just radiation for the vacuum situation. All models include conduction through the glass cover, and convection and radiation off the top surface.
- **2D simulation to show heat transfer out of the device:** This 2D simulation is an extension of the 1D calculations, but it allows the temperature gradient effects on heat loss to be analyzed as well.
- **3D periodic simulation showing heat lost through a system with an infinite number of cycles:** By including one serpentine cycle with periodic heat boundary conditions on each side, the fluid carrying heat both up and down the height of the device is included in the analysis to give a comprehensive analysis of the system assuming there were an infinite number of serpentine cycles. This model is very important as it includes all the heat transfer present, ignoring only end effects.
- **CF-PCR experimental platform:** The experimental setup was designed and machined for this particular device. It includes the Teflon base, PC cover, two black spray-painted glass slides, two heaters and two temperature sensors.
- **PC channel manufacturing protocol:** The protocol for manufacturing the PC devices using the laser cutting technique was developed. The laser settings and heat press parameters were all optimized to produce the most accurate device with smooth edges and minimal bubbles in the final product.

- **PC channel cleaning protocol:** Although the device is considered disposable, it can be reused assuming the appropriate cleaning protocol is followed. The volume and flow rates for the various solutions in the cleaning protocol have been determined.

6.3 Future Work

Although significant headway has been made in the development of this device, further work is necessary to decrease the cycle time and solve the flow rate problems during experimentation before this device could be used in industry.

- **Change channel geometry to increase cycle time:** The current design features an elegant design which is capable of performing PCR on a DNA segment of variable length. It has been shown to be effective at flow rates of 0.5 mL/hr or less, resulting in a cycle time of 30 seconds and a total reaction time of 13.4 minutes. If the DNA segment length is known, the width of the channel during the extension phase could be modified to allow the sample to remain in the extension temperature limits for only the time required for the length of DNA segment. In essence, the channel width would be mostly constant throughout the channel with the exception of a small increase in width designed to be centered around the 72°C point in the temperature gradient.
- **Improve flow rate during experiments:** A large problem experienced during experimentation was an inconsistent flow rate. It has been suggested that pushing the sample through the channel, opposed to pulling it, would produce a more predictable flow rate due to the larger potential pressure difference. Another

suggested method for creating a consistent flow rate is by using a smaller syringe. Syringe pumps calculate the distance the syringe head must travel based on the syringe diameter and user-defined volumetric flow rate. In general, syringe pumps are able to constantly move the syringe head to achieve the desired flow rate. However, for slow flow rates and large syringes, the pump is limited by the minimum distance it is able to move. If the distance calculated is smaller than the minimum travel distance of the pump, the pump moves the minimum distance then stalls to compensate. This abrupt start and stop behavior is another potential cause of inconsistent flow rates. If a smaller diameter syringe is used, this behavior may be eliminated.

- **Find optimal heater temperature set-point for 1 mL/hr:** Assuming the flow rate is consistent, an experiment must be completed to determine the optimal heater temperature set-points for a flow rate of 1 mL/hr. With the flow rate abnormalities experienced during testing, a successful combination of heater temperatures was not found. With a more predictable flow rate, this test is expected to be successful.
- **Perform fluorescence while PCR is occurring:** The PCR analysis was performed after the sample had been removed from the channel; however, this device is capable of real-time fluorescence imaging. By incorporating this analysis in the experiment, the amplification through each cycle could be observed.

6.4 Summary

A polycarbonate device has been designed, simulated, manufactured and tested to achieve PCR reaction temperatures successfully. Simulations have been developed which accurately represent the device in a lab setting and can be trusted in future work.

REFERENCES

[1] S. D. J. Pena and R. Chakraborty, "Paternity testing in the DNA era," Trends in Genetics, vol. 10, pp. 204-209, 1994.

[2] S. I. Makino, et al., "Detection of anthrax spores from the air by real-time PCR," Letters in Applied Microbiology, vol. 33, pp. 237-240, 2001.

[3] H. Cheun, et al., "Rapid and effective detection of anthrax spores in soil by PCR," Journal of Applied Microbiology, vol. 95, pp. 728-733, 2003.

[4] H. A. Erlich, "PCR Technology: Principles and Applications for DNA Amplification," 1992 ed. New York: W.H. Freeman and Company, 1992, p. 11.

[5] S. A. Bustin, The PCR Revolution: Basic Technologies and Applications. New York: Cambridge University Press, 2010.

[6] C. Wittwer, et al., "Automated polymerase chain reaction in capillary tubes with hot air," Nucleic Acids Research, vol. 17, p. 4353, 1989.

[7] S. R. Beard, et al., "Microwell Array PCR Chip for Study of Genetically Engineered Mouse Stem Cells," presented at the MicroTAS 2011, Seattle, Washington, 2011.

[8] M. A. Shoffner, et al., "Chip PCR. I. Surface passivation of microfabricated silicon-glass chips for PCR," Nucleic Acids Research, vol. 24, p. 375, 1996.

[9] Y. Ouyang, et al., "Development of Disposable Multichambered Microchip PCR Via Non-Contact IR Mediated Thermal Control," presented at the MicroTAS 2011, Seattle, Washington, 2011.

[10] J. A. Lounsbury, et al., "A Multi-Chamber PMMA Microdevice for Simultaneous Amplification of up to Sevel Individual Samples Using Infrared-Mediated PCR," presented at the MicroTAS 2011, Seattle, Washington, 2011.

[11] A. Hühmer and J. Landers, "Noncontact infrared-mediated thermocycling for effective polymerase chain reaction amplification of DNA in nanoliter volumes," Analytical Chemistry, vol. 72, pp. 5507-5512, 2000.

[12] R. Oda, et al., "Infrared-mediated thermocycling for ultrafast polymerase chain reaction amplification of DNA," Analytical Chemistry, vol. 70, pp. 4361-4368, 1998.

[13] M. Kanai, et al., "A Novel Contamination Free PCR Well Array Device for Clinical Applications," presented at the MicroTAS 2011, Seattle, Washington, 2011.

[14] T. M. H. Lee, et al., "Microfabricated PCR-electrochemical device for simultaneous DNA amplification and detection," Lab on a Chip, vol. 3, pp. 100-105, 2003.

[15] L. Chen, et al., "Ultrasensitive PCR and real-time detection from human genomic samples using a bidirectional flow microreactor," Analytical Chemistry, vol. 79, pp. 9185-9190, 2007.

[16] J. Chiou, et al., "A closed-cycle capillary polymerase chain reaction machine," Analytical Chemistry, vol. 73, pp. 2018-2021, 2001.

[17] J. Y. Cheng, et al., "Performing microchannel temperature cycling reactions using reciprocating reagent shuttling along a radial temperature gradient," Analyst, vol. 130, pp. 931-940, 2005.

[18] M. U. Kopp, et al., "Chemical amplification: continuous-flow PCR on a chip," Science, vol. 280, p. 1046, 1998.

[19] I. Schneega, et al., "Miniaturized flow-through PCR with different template types in a silicon chip thermocycler," Lab on a Chip, vol. 1, pp. 42-49, 2001.

[20] S. Li, et al., "A continuous-flow polymerase chain reaction microchip with regional velocity control," Microelectromechanical Systems, Journal of, vol. 15, pp. 223-236, 2006.

[21] M. Hashimoto, et al., "Rapid PCR in a continuous flow device," Lab Chip, vol. 4, pp. 638-645, 2004.

[22] N. Park, et al., "Cylindrical compact thermal-cycling device for continuous-flow polymerase chain reaction," Analytical Chemistry, vol. 75, pp. 6029-6033, 2003.

[23] K. D. Dorfman, et al., "Contamination-free continuous flow microfluidic polymerase chain reaction for quantitative and clinical applications," Analytical Chemistry, vol. 77, pp. 3700-3704, 2005.

[24] J. Chen, et al., "Electrokinetically synchronized polymerase chain reaction microchip fabricated in polycarbonate," Analytical Chemistry, vol. 77, pp. 658-666, 2005.

[25] C. T. Wittwer and M. G. Herrmann, "Rapid thermal cycling and PCR kinetics," PCR applications: protocols for functional genomics, p. 211, 1999.

[26] N. D. Crews Jr, "Continuous-flow temperature gradient microfluidics: Spatial polymerase chain reaction and melting analysis," The University of Utah, 2009.

[27] R. L. Orozco, "Computational Heat Transfer Study of Thermal Gradient Continuous Flow Polymerase Chain Reaction Devices," Department of Mechanical Engineering, University of Utah, 2009.

[28] N. Crews, et al., "Continuous-flow thermal gradient PCR," Biomedical microdevices, vol. 10, pp. 187-195, 2008.

[29] Y. Chen, et al., "Silicate polymerization for the preparation of bed-retention frits in capillary electrochromatography," Analytical Chemistry, vol. 72, pp. 610-615, 2000.

[30] Q. Q. Cao, et al., "Plastic microfluidic chip for continuous flow polymerase chain reaction: Simulations and experiments," Biotechnology journal, 2010.

[31] Y. S. Shin, et al., "PDMS-based micro PCR chip with parylene coating," Journal of Micromechanics and Microengineering, vol. 13, p. 768, 2003.

[32] J. A. Kim, et al., "Fabrication and characterization of a PDMS-glass hybrid continuous-flow PCR chip," Biochemical engineering journal, vol. 29, pp. 91-97, 2006.

[33] N.-T. Nguyen and S. Wereley, Fundamentals and Applications of Microfluidics, 2 ed.: Artech House, 2006.

[34] Y. Cengel and J. Cimbala, Fluid Mechanics Fundamentals and Applications: McGraw Hill, 2006.

[35] F. Incropera, et al., Fundamentals of Heat and Mass Transfer, 6 ed., 2007.

[36] T. Nakayama, et al., "Circumventing air bubbles in microfluidic systems and quantitative continuous-flow PCR applications," Anal Bioanal Chem, pp. 1327-1333, 2006.